A Concerted Mechanism Involving ACAT and SREBPs By which Oxysterols Deplete Accessible Cholesterol To Restrict Microbial Infection

David B. Heisler[1,3], Kristen A. Johnson[2,3,4], Maikke B. Ohlson[1], Duo Ma[1,2], Lishu Zhang[1], Michelle Tran[2], Chase D. Corley[2], Michael E. Abrams[1], Jeffrey G. McDonald[2], John W. Schoggins[1], Neal M. Alto[1,*], and Arun Radhakrishnan[2,5,*]

[1] Department of Microbiology, The University of Texas Southwestern Medical Center, Dallas, TX 75390, USA
[2] Department of Molecular Genetics, The University of Texas Southwestern Medical Center, Dallas, TX 75390, USA
[3] These authors contributed equally to this manuscript.
[4] Current affiliation: Fred Hutchinson Cancer Center, Clinical Research Division, Seattle WA.
[5] Lead Contact
[*] Corresponding Authors:
neal.alto@utsouthwestern.edu and arun.radhakrishnan@utsouthwestern.edu

Abstract

Most of the cholesterol in the plasma membranes (PMs) of animal cells is sequestered through interactions with phospholipids and transmembrane domains of proteins. However, as cholesterol concentration rises above the PM's sequestration capacity, a new pool of cholesterol, called accessible cholesterol, emerges. The transport of accessible cholesterol between the PM and the endoplasmic reticulum (ER) is critical to maintain cholesterol homeostasis. This pathway has also been implicated in the suppression of both bacterial and viral pathogens by immunomodulatory oxysterols. Here, we describe a mechanism of depletion of accessible cholesterol from PMs by the oxysterol 25-hydroxycholesterol (25HC). We show that 25HC-mediated activation of acyl coenzyme A: cholesterol acyltransferase (ACAT) in the ER creates an imbalance in the equilibrium distribution of accessible cholesterol between the ER and PM. This imbalance triggers the rapid internalization of accessible cholesterol from the PM, which is sustained for long periods of time through 25HC-mediated suppression of SREBPs. In support of a physiological role for this mechanism, 25HC failed to suppress Zika virus and human coronavirus infection in ACAT-deficient cells, and *Listeria monocytogenes* infection in ACAT-deficient cells and mice. We propose that selective depletion of accessible PM cholesterol triggered by ACAT activation and sustained through SREBP suppression underpins the immunological activities of 25HC and a functionally related class of oxysterols.

Introduction

Cholesterol is an essential component of the membranes of animal cells and its levels are tightly regulated by multiple feedback mechanisms that control its production, uptake, and intracellular distribution (1, 2). Dysregulation of cellular cholesterol homeostasis is implicated in many human diseases ranging from atherosclerosis to cancer (3, 4). There is also growing evidence that membrane cholesterol modulation plays key roles in host defense against bacterial and viral pathogens (5-8). While the proteins and pathways that mediate cholesterol regulation have been extensively studied, how these processes are rapidly altered during infection remains poorly defined.

Most of a mammalian cell's cholesterol is concentrated in the plasma membrane (PM), where the molecule makes up 40 – 50% of the total lipids (9). The steady state levels of PM cholesterol are regulated by balancing the flow of cholesterol into and out of the PM. Inflows to the PM originate from two locations – i) the endoplasmic reticulum (ER) where cholesterol is synthesized; and ii) lysosomes where cholesterol is liberated from low-density lipoproteins (LDL) that bind to LDL receptors on the PM and are internalized by receptor-mediated endocytosis (10). Upon arrival at the PM from these locations, the incoming cholesterol forms complexes with sphingomyelin (SM) and other PM phospholipids, which imparts the PM with structural properties required for proper cellular function and growth (11, 12). Cholesterol in excess of the sequestering capacity of PM phospholipids forms a pool that has been termed "accessible cholesterol" (13). Expansion of this pool signals cholesterol overaccumulation and triggers flow of accessible cholesterol out of the cell by PM cholesterol efflux proteins (14, 15), or into the cell by cholesterol transporters that move the lipid to organelles such as the ER (16, 17).

The accessible cholesterol that is transported to the ER interacts with two regulatory membrane proteins, a cholesterol sensor called Scap (18, 19) and a cholesterol-modifying enzyme called acyl coenzyme A: cholesterol acyltransferase (ACAT) (20, 21). Binding of cholesterol to Scap prevents the activation of sterol regulatory element-binding proteins (SREBPs), transcription factors that upregulate genes for lipid production, including those for cholesterol synthesis and uptake (1). The ACAT enzyme converts some of the incoming cholesterol to cholesteryl esters for storage in cytoplasmic lipid droplets (22). Thus, the transcriptional and enzymatic responses induced by accessible cholesterol arriving at the ER combine to reduce cellular cholesterol and protect the PM from cholesterol overaccumulation.

While accessible cholesterol in the PM plays a crucial role in maintaining cholesterol homeostasis and regulating cell growth, this pool of cholesterol can also be a vulnerability as it is exploited by numerous bacteria and viruses to promote infection (6-8). Fortunately, animal cells have devised a clever solution to rectify this vulnerability. The solution involves an innate immune response that stimulates the expression of cholesterol 25-hydroxylase (CH25H), an enzyme that attaches a hydroxyl group to the iso-octyl sidechain of cholesterol to generate 25-hydroxycholesterol (25HC), a potent signaling molecule (23). 25HC produced by macrophage cells in response to infection acts in a paracrine manner to induce rapid depletion of accessible cholesterol, but not cholesterol in complexes with SM, from the PMs of nearby cells. Such depletion prevents the spread of infection by bacterial pathogens such as *Listeria monocytogenes* and *Shigella flexneri* (6) as well as cellular infection by viruses such as SARS-CoV-2, the causative agent of COVID-19 (8). In addition, 25HC acts in an autocrine manner to prevent macrophage lysis by bacterial pore-forming toxins that target accessible cholesterol in membranes (7).

Establishing the mechanisms of how 25HC rapidly depletes accessible cholesterol from PMs has been complicated due to this oxysterol's actions on multiple cholesterol homeostatic pathways, including *i*) binding to Insigs, which suppresses the activation of SREBPs and reduces cholesterol synthesis and uptake (24); *ii*) activating Liver X receptors (LXRs), transcription factors that upregulate genes encoding proteins involved in cholesterol efflux (14, 25); and *iii*) stimulating the activity of ACAT, which esterifies cholesterol (22, 26). Each of these actions would lower levels of total cellular cholesterol, which would then be expected to lower accessible cholesterol in PMs. The recent studies on 25HC's role in restricting pathogen infection (6-8) have pointed to the involvement of two of these pathways - ACAT and SREBP - in depleting accessible cholesterol from PMs, however several questions remain unanswered. First, what is the primary target of 25HC that initiates depletion of accessible cholesterol from the PM? Second, what is the underlying mechanism by which 25HC depletes PMs of accessible cholesterol? Third, how does 25HC sustain low levels of accessible PM cholesterol over long time periods necessary to disrupt the lifecycles of pathogens *in vivo*? Finally, does 25HC inhibit both bacterial and viral infections through a common mechanism?

Here, using a panel of oxysterols with diverse structures and cell lines deficient in key components that regulate cholesterol homeostasis, we find that rapid depletion of accessible cholesterol from PMs by 25HC is solely determined by ACAT activity. Stimulation of ACAT by 25HC siphons off cholesterol that arrives at the ER for conversion to cholesteryl esters, forcing a

redistribution of cellular cholesterol, which ultimately leads to a decrease in accessible PM cholesterol. Once initiated through ACAT, the depletion of accessible PM cholesterol persists for longer periods through 25HC's inhibition of transcriptional pathways responsible for cholesterol synthesis and uptake. In the absence of ACAT, 25HC no longer protects cells from lysis by cytolysins secreted by *Clostridium perfringens* and *Bacillus anthracis*, infection by *Listeria monocytogenes*, or infection by Zika virus and coronaviruses. Moreover, in an ACAT-deficient animal model, 25HC-mediated protection of the spleen and liver from infection by *Listeria monocytogenes* is reduced. Together, these studies unite the disparate reports of anti-bacterial and anti-viral properties of 25HC through a common mechanism orchestrated by ACAT.

Results

Side-chain oxysterols like 25HC trigger rapid depletion of accessible cholesterol from PMs

To carry out a detailed examination of the effects of 25HC on PM cholesterol, we chose Chinese hamster ovary (CHO) cells as a model cellular system since these cells have been used for more than two decades to study cholesterol regulatory pathways (22, 27). To detect accessible cholesterol in PMs of live cells, we used domain 4 of anthrolysin O (ALOD4), a non-lytic protein sensor that specifically detects this pool of cholesterol in membranes (***Figure S1A***) (17, 28). When a line of CHO cells designated CHO-K1 were grown in cholesterol-rich fetal calf serum (FCS), their PMs contained high levels of accessible cholesterol that were readily detected by ALOD4 (***Figures 1A & 1B****, lane 1 of top panels*). When these cells were incubated with 25HC for increasing times, ALOD4 binding declined sharply after 1 hour and was eliminated after 4 hours (***Figure 1A****, top panel*). When treated with increasing concentrations of 25HC, ALOD4 binding was sharply reduced after treatment with 1 μM 25HC and eliminated when 25HC exceeded 2.5 μM (***Figure 1B****, top panel*). Thus, treatment of CHO-K1 cells with 25HC rapidly depleted accessible cholesterol from PMs in a dose-dependent manner, as observed previously in other cell types (6, 7).

We next asked whether 25HC was unique among oxysterols in triggering such rapid depletion of accessible PM cholesterol. To address this question, we assayed a panel of structurally diverse oxysterols (***Figure 1C***) harboring hydroxyl groups on the steroid nucleus (*A* – *C*) or the iso-octyl side-chain (*D* – *J*), as well as an oxysterol where the 3β-hydroxyl was replaced with a sulfate group (*K*). As shown in ***Figure 1D***, ALOD4 binding to the PMs of CHO-K1 cells was markedly reduced by treatment for 4 hours with 25HC (*I*), as well as oxysterols harboring hydroxyl groups at carbons 20 (*D*) or 27 (*J*). Oxysterols with hydroxyl groups at carbon 24 (*G*, *H*) partially reduced ALOD4 binding, whereas oxysterols with hydroxyl groups on carbon 22 (*E*, *F*)

had no effect. These data indicate that the location of the hydroxyl modification on the sterol side-chain plays a crucial role in controlling accessible PM cholesterol. Moreover, the ability of a side-chain oxysterol like 25HC (*I*) to reduce ALOD4 binding required the 3β-hydroxyl group since replacement of this group with a sulfate group (*K*) abolished this effect. No reduction of ALOD4 binding was detected with oxysterols bearing hydroxyl groups on the steroid nucleus at carbons 4 (*A*), 7 (*B*), or 19 (*C*). While oxysterols *D, G, H, I,* and *J* reduced ALOD4 binding in an all-or-none fashion, they had no detectable effect on the binding of Ostreolysin A (OlyA) (***Figure 1E***), a sensor for the SM-sequestered pool of PM cholesterol (***Figure S1A***) (29, 30). In line with the immunoblot analysis in ***Figures 1D & E***, microscopy imaging with fluorescent versions of ALOD4 (fALOD4-Neon) and OlyA (fOlyA-647) also showed that oxysterols *D*, *G*, *H*, *I*, and *J* eliminated accessible cholesterol, but not SM-sequestered cholesterol, from the PMs of CHO-K1 cells (***Figure S1B***).

We followed up with dose curve analysis of the effect of each oxysterol on ALOD4 binding. At the highest concentrations tested, oxysterols *D*, *G*, *H*, *I*, and *J* reduced ALOD4 binding by more than 65%, whereas treatment with oxysterols *A*, *B*, *C*, *E*, *F*, or *K* showed no such reduction (***Figure S1C***). Detailed time course analyses for the five oxysterols that markedly reduced ALOD4 binding (*D*, *G*, *H*, *I*, and *J*) showed that oxysterols *D*, *I*, and *J* reduced binding by more than 50% within 1 hour, whereas oxysterols *G* and *H* required 4 hours for a similar reduction (***Figure S1D***). Together, these data indicate that selective depletion of accessible PM cholesterol within 4 hours is triggered by oxysterols harboring hydroxyl groups on the iso-octyl side chain at carbons 20, 24, 25, or 27.

To support our interpretation that the reduction of ALOD4 binding by certain oxysterols indicated depletion of accessible PM cholesterol, we carried out flow cytometry analysis of fALOD4-Neon binding to rabbit red blood cells (RBCs), which have an outer limiting membrane with high levels of accessible cholesterol but no internal membranes or mechanisms to synthesize, modify, or internalize cholesterol (31). As shown in ***Figures S2A*** and ***S2B***, We observed no reduction in fALOD4-Neon binding to RBCs that were treated for 4 hours with the panel of oxysterols (***Figure 1C***), whereas binding was abolished by treatment with hydroxypropyl β-cyclodextrin (HPCD), a reagent that extracts cholesterol from membranes (32). These results suggest that reduction of ALOD4 binding to the PMs of CHO-K1 cells by oxysterols *D*, *G*, *H*, *I*, and *J* is not due to effects on the lipid bilayer or on ALOD4, but rather due to their effects on cholesterol homeostatic pathways.

Stimulation of ACAT activity triggers rapid depletion of accessible cholesterol from PMs

Oxysterols lower cellular cholesterol by targeting multiple cholesterol homeostatic systems, including ACAT, SREBPs, and LXRs. Having established which oxysterols rapidly deplete accessible PM cholesterol (***Figure 1D***), we sought to determine if one or more of these cholesterol homeostatic systems are regulated by the same oxysterols. We first tested the oxysterol specificity for activation of ACAT's enzymatic activity using a well-established cellular assay that measures ACAT's ability to attach [^{14}C]oleate, a radiolabeled fatty acid, to cholesterol to generate cholesteryl [^{14}C]oleate (33). In the absence of oxysterol treatment, ACAT activity in CHO-K1 cells was low (***Figure 1F***, *column 1*). Oxysterols *D*, *G*, *H*, *I*, and *J* stimulated a more than six-fold increase in ACAT activity, whereas oxysterols *A*, *B*, *C*, *E*, *F*, and *K* did not show a similar stimulatory effect (***Figure 1F***). This specificity for activation of ACAT exactly matched that for the depletion of accessible cholesterol from PMs (***Figure 1D***).

We then assessed the oxysterol specificity for inactivation of SREBPs with an assay that we routinely use to monitor the status of SREBP2, one of the three isoforms of SREBP (24, 34). In this experiment, CHO-K1 cells were first depleted of cholesterol by treatment with HPCD, which triggered the conversion of SREBP2 from its inactive precursor form (*P*) to its active cleaved nuclear form (*N*) (***Figure 1G***, *lane 1*). When the cholesterol-depleted cells were then treated with each of the oxysterols for 4 hours, we observed that oxysterols *B*, *D*, *E*, *G*, *H*, *I*, *J*, and *K* suppressed SREBP2 cleavage whereas oxysterols *A*, *C*, and *F* had a reduced effect (***Figure 1G****, lanes 2- 12*). This specificity profile did not match that for depletion of accessible cholesterol from PMs (see summary table in ***Figure 1H***). In particular, oxysterols *B*, *E*, and *K* suppressed SREBP2 cleavage but were unable to reduce ALOD4 binding (***Figure 1D***), suggesting that SREBP2 suppression does not drive the rapid depletion of accessible cholesterol from PMs.

Lastly, we evaluated the extensive previous literature that has addressed the oxysterol specificity for activating LXR transcription factors (25, 35-39). These studies showed that oxysterols *A*, *B*, *E*, *G*, *H*, *I*, and *J* activate LXRs whereas oxysterols *F* and *K* had no such activating effect (see summary table in ***Figure 1H***). Similar to results with SREBP2, the oxysterol specificity for LXR activation also did not match that for reduction in ALOD4 binding.

Disruption of ACAT activity abolishes the ability of oxysterols to rapidly deplete accessible cholesterol from PMs

The above oxysterol specificity analysis suggested that ACAT, but not SREBPs or LXRs, triggers the rapid depletion of accessible PM cholesterol. To test this hypothesis, we generated a CHO-K1 cell line that lacks ACAT enzymatic activity. Mammalian cells contain two isoforms of ACAT, ACAT1 and ACAT2, however previous studies of CHO cells have shown that ~99% of

their ACAT activity arises from the ACAT1 isoform (40, 41). Therefore, we used CRISPR-Cas9 genome editing to disrupt the ACAT1 gene in CHO-K1 cells (***Figure S3A***). The resulting ACAT1-deficient cells, hereafter designated as ACAT1$^{-/-}$ cells, had undetectable levels of ACAT1 protein (***Figure S3B***). Moreover, ACAT enzymatic activity, as judged by cholesteryl[^{14}C]oleate formation, was stimulated by 25HC, one of the five oxysterols that triggered ACAT activity (***Figure 1F***), to an expected degree in wild-type (WT) cells but not in ACAT1$^{-/-}$ cells (***Figure S3D***, *first two groups*), further indicating that the ACAT1$^{-/-}$ cells lacked ACAT activity. To ensure that these results were due to loss of ACAT activity, we stably expressed either wild-type human ACAT1 or a mutant version harboring a point mutation (H460A) that abolishes ACAT1's enzymatic activity in ACAT1$^{-/-}$ cells, and the resulting cell lines were designated as ACAT1$^{-/-}$; hACAT1(WT) and ACAT1$^{-/-}$; hACAT1(H460A), respectively. Compared to the ACAT1$^{-/-}$ cells, these two new cell lines contained high levels of ACAT1 protein (***Figure S3C***). Moreover, stimulation of ACAT enzymatic activity by 25HC was restored by the stable expression of hACAT1(WT), but not hACAT1(H460A) (***Figure S3D,*** *last two groups*). Thus, these four cell lines provide a framework to study the specific role of ACAT activity in determining accessible cholesterol levels in PMs.

We then measured the effects of 25HC on accessible cholesterol cholesterol in the PMs of these four cell lines. As expected, treatment of WT cells with 25HC for 4 hours depleted PM accessible cholesterol in a dose-dependent manner (***Figure 2A***, *lanes 1 – 6*, *first panel*). In contrast, no such depletion was observed in ACAT1$^{-/-}$ cells (***Figure 2A***, *lanes 1 – 6, third panel*). Restoration of ACAT activity by stable expression of hACAT1(WT) reestablished the ability of 25HC to deplete accessible PM cholesterol, whereas 25HC had no effect in cells stably expressing an inactive mutant of hACAT1 (H460A) (***Figure 2A***, *lanes 1 – 6, fifth and seventh panels*). When each of these four cell lines were depleted of sterols and then treated with 25HC, we observed similar dose dependences for suppression of SREBP2 processing (***Figure S4***), indicating that 25HC entered the cells and reached their ER membranes to bind Insigs and prevent SREBP2 transport. Thus, the inability of 25HC to deplete accessible PM cholesterol in ACAT1$^{-/-}$ cells is not simply due to a defect in cellular entry of 25HC. In all four cell lines, 4HC did not diminish PM accessible cholesterol (***Figure 2A***, *lane 7, all panels*), consistent with this oxysterol's inability to stimulate ACAT activity (***Figure 1F****, oxysterol A*). Similar to the results with 25HC, the 4 other oxysterols that depleted accessible PM cholesterol in WT cells (***Figure 1F***, *oxysterols D, G, H, and J*) were also unable to do so in the ACAT1$^{-/-}$ cells, further underscoring the link between ACAT and accessible PM cholesterol (***Figure S5***).

We also used fluorescence microscopy to analyze the effects of 25HC on the distribution of accessible and SM-sequestered pools of cholesterol in these cell lines. Consistent with

immunoblot analysis (***Figure 2A***), we observed that 25HC treatment for 4 hours eliminated binding of fALOD4-Neon to WT cells, and this effect was abolished in ACAT1$^{-/-}$ cells (***Figure 2B***, *top two rows*). Likewise, expression of hACAT1(WT), but not hACAT1(H460A), in the ACAT1$^{-/-}$ cells restored 25HC's ability to deplete fALOD4-Neon binding (***Figure 2B***, *third and fourth rows*). In all four cell lines, binding of fOlyA-647 was unchanged by 25HC treatment (***Figure 2B***), further highlighting that over a period of 4 hours, 25HC specifically depletes the accessible pool of PM cholesterol in an ACAT-mediated manner.

To confirm that ACAT is the primary target of 25HC for rapid depletion of accessible PM cholesterol, we examined two previously described cell lines, one lacking all three isoforms of SREBPs (owing to a deficiency of Scap, which stabilizes SREBPs) (42, 43) and the other lacking both isoforms of LXRs (6). Compared to WT cells, Scap-deficient cells (that have no detectable SREBPs) and LXR-deficient cells both had lower levels of accessible cholesterol on their PMs (***Figure 2C*** and ***2D***, *left panels*, *lane 1*), and this pool of cholesterol was completely depleted by treatment with 25HC for 4 hours (*lanes 2 – 6*). Treatment with 4HC had no effect on accessible cholesterol levels in either Scap- or LXR-deficient cells (***Figure 2C*** and ***2D***, *left panels*, *lane 7*). Also, levels of SM-sequestered cholesterol in these cells were unchanged after treatment with either 25HC or 4HC (***Figure 2C*** and ***2D***, *right panels*, *lanes 1 – 7*).

Combined, the above sets of studies show that the rapid (1–4 hours) removal of accessible cholesterol from PMs by 25HC is due to its activation of ACAT and not due to its modulation of the SREBP or LXR pathways.

A model for rapid depletion of accessible cholesterol from PMs by ER-localized ACAT

The concentration of cholesterol in the PM (~40-50 mole% of total lipids) is almost 10-fold higher than that in the ER membrane (~5 mole% of total lipids) (44-46). How then can activation of ACAT, a cholesterol-modifying enzyme in the ER membrane, rapidly alter the levels of the accessible cholesterol pool in the PM? Previous studies have suggested that even though the total cholesterol concentrations in the PM and ER are quite different, the concentration of accessible cholesterol in the two membranes may be similar (47, 48). The equivalence in accessible cholesterol levels between the PM and ER is maintained by rapid bi-directional transport of cholesterol between the two membranes (49). Based on these previous insights, we propose that ACAT activation, and the resulting production of cholesteryl esters, would siphon off some of the accessible cholesterol from the ER, thus lowering levels of accessible cholesterol in the ER relative to the PM. Cholesterol transport from the PM to the ER would then rapidly restore

the equivalence of accessible cholesterol between the two membranes. As a result, levels of accessible cholesterol in the PM would decline.

The above model provides a possible explanation for how ACAT activation by 25HC would lead to a depletion of accessible PM cholesterol in WT cells, but not in ACAT1$^{-/-}$ cells (***Figure 2A***). We further tested this model by activating ACAT not by 25HC but by lipoproteins, which have been shown to generate high ACAT activity (33). We then took advantage of the sensitivity of flow cytometry analysis to assess levels of accessible and SM-sequestered cholesterol in the PMs of WT and ACAT1$^{-/-}$ cells with fluorescent versions of ALOD4 and OlyA, respectively. When cells are grown under low cholesterol conditions (lipoprotein-deficient serum, LPDS), ACAT activity is low (33). Under these conditions, both WT and ACAT1$^{-/-}$ cells had the same low levels of accessible and SM-sequestered cholesterol in their PMs (***Figure 3A***). By comparison, when cells are grown under high cholesterol conditions (FCS), ACAT activity is high (33). In this case, the PMs of ACAT1$^{-/-}$ cells had significantly higher levels of accessible cholesterol as compared to WT cells (***Figure 3B***). This result is consistent with the model proposed above since the ACAT1$^{-/-}$ cells, unlike the WT cells, are unable to siphon away ER cholesterol, leading to higher levels of accessible cholesterol in the PMs of these cells. Importantly, there was no difference in levels of SM-sequestered cholesterol in the PMs of WT and ACAT1$^{-/-}$ cells (***Figure 3B***), highlighting the specific effect of the ACAT pathway on accessible PM cholesterol.

An assumption of our model is that rapid bi-directional transport of accessible cholesterol between the PM and the ER was not disrupted in ACAT1$^{-/-}$ cells. To test this notion, we carried out three different experiments in which the cholesterol content of the PM was varied and changes in ER cholesterol were monitored by assessing the molecular size of SREBP2, which is processed from its precursor form (*P*) to a cleaved nuclear form (*N*) in response to decreases in ER cholesterol (46). First, we depleted cholesterol from the PMs of FCS-treated cells by incubation with HPCD, which extracts cholesterol from PMs. The reduction in PM cholesterol is rapidly compensated for by drawing cholesterol from the ER, leading to a reduction in ER cholesterol levels and an increase in SREBP2 cleavage. In both WT and ACAT1$^{-/-}$ cells, HPCD treatment reduced ER cholesterol levels with similar time dependences (***Figure 3C***), indicating that the pathways that transport cholesterol from ER to PM are not affected in the ACAT1$^{-/-}$ cells.

Second, we depleted both cell lines of cholesterol by incubation overnight in the presence of lipoprotein-deficient serum along with compactin, an inhibitor of cholesterol synthesis (50). This treatment lowered ER cholesterol to a similar degree in both cell lines, as judged by similar levels of nuclear SREBP2 (***Figure 3D***, *lane 1*, *first and third panels*). We then added back increasing concentrations of lipoprotein-rich FCS and observed a similar dose-dependent increase in ER

cholesterol in both cell lines, as judged by reduction of nuclear SREBP2 (***Figure 3D***, *lanes 2 – 7*). Third, we depleted cells of cholesterol by treatment with HPCD and then added back increasing concentrations of complexes of cholesterol with methyl-β-cyclodextrin (MCD), which deliver cholesterol to the PMs. Analysis of SREBP2 cleavage in both cell lines showed similar reduction in ER cholesterol levels upon depletion (***Figure 3E***, *lane 1*, *first and third panels*), and a similar dose-dependent increase in ER cholesterol levels upon replenishment with cholesterol/MCD (***Figure 3E***, *lanes 2 – 6*). The results of ***Figures 3D*** and ***3E*** suggest that the pathways transporting lipoprotein-derived or exogenously added cholesterol from PM to ER are not affected in the ACAT1$^{-/-}$ cells.

Taken together, the results in ***Figure 3*** provide a plausible mechanism for how 25HC and other ACAT-activating oxysterols could rapidly alter the levels of accessible cholesterol in the PMs of cells whose overall cholesterol content varies over a wide range.

25HC-triggered depletion of accessible PM cholesterol persists long after 25HC removal through suppression of SREBPs

We next wondered whether the rapid depletion of accessible PM cholesterol after a short exposure to 25HC would be sustained over longer periods. To explore this possibility, we first treated CHO-K1 cells with 25HC for a short period of 4 hours, which depleted accessible cholesterol from the PMs in an expected manner (***Figure 4A***, *first panel*, *lanes 1, 2*). We then removed the 25HC and examined accessible PM cholesterol levels over time. Despite the lack of 25HC in the extracellular media and cells being grown in cholesterol-rich FCS, we detected no replenishment of accessible PM cholesterol even after 22 hours (***Figure 4A***, *first panel*, *lanes 3 – 8*). In line with our model of equivalence of accessible cholesterol levels in the PM and ER (***Figure 3A***), we expected that ER accessible cholesterol levels would also be low 22 hours after 25HC removal, which would be reflected in increased cleavage of SREBP2 to its nuclear form. Surprisingly, we detected no processing of SREBP2 (***Figure 4A***, *third panel*). Mass spectrometric analysis of intracellular 25HC levels (***Figure 4A***, *bottom panel*) showed that 25HC was barely detectable (~0.015 ng/μg of cellular protein) in untreated cells (*lane 1*) and rose to 4 ng/μg of cellular protein after 25HC treatment for 4 hours (*lane 2*). After removal of 25HC from the extracellular medium, the intracellular 25HC declined over the time course of 22 hours to 0.35 ng/μg of cellular protein (*lanes 3 – 8*), a level that was 23-times higher than that in untreated cells and sufficient to suppress SREBP2 cleavage (***Figure 4A****, lane 8*).

In contrast to the sustained action of 25HC, when accessible PM cholesterol was depleted by treatment with HPCD (1 hour), its levels were replenished within 4 hours of HPCD removal

(***Figure 4B***, *first panel*). Moreover, HPCD depletion triggered SREBP2 cleavage in an expected fashion (***Figure 4B***, *second panel*, *lanes 1, 2*), and this cleavage was suppressed at the same time as an increase in PM accessible cholesterol was detected (***Figure 4B***, *second panel, lanes 3 – 8*). These data further support the notion that 25HC's long-term effects arise due to its suppression of SREBP cleavage. If this was the case, we would expect 25HC's effects to be overcome by expression of the cleaved nuclear forms of SREBPs. We tested this possibility in previously developed cell lines where expression of the cleaved nuclear forms of each of the three isoforms of SREBPs – SREBP1a, SREBP1c, and SREBP2 – can be induced by addition of the small molecule muristerone (51). In the absence of muristerone, these cells had detectable levels of accessible cholesterol in their PMs (***Figure 4C***, *lane 1*). 25HC treatment depleted this pool and no replenishment was observed 22 hours after the 25HC (***Figure 4C***, *lanes 2, 3*). We then treated the cells with muristerone to induce the expression of the nuclear forms of each of the three SREBPs (***Figure 4C***, *lanes 4 – 6*). Under these conditions, the accessible cholesterol in the PMs of these cells was also depleted by 25HC (***Figure 4C***, *lanes 4, 5*). However, when the 25HC was removed, we now detected replenishment of accessible cholesterol on the PMs of cells expressing the nuclear forms of SREBP1a and SREBP2, but not SREBP1c (***Figure 4C***, *lane 6*). This isoform specificity for restoring accessible PM cholesterol is consistent with the previous observation that the nuclear forms of SREBP1a and SREBP2, but not SREBP1c, increase cholesterol synthesis and induce expression of the LDL receptor allowing for uptake of cholesterol from the LDL in FCS (51).

Based on these data, we hypothesized that 25HC acts through two distinct, temporally resolved stages. First, a short pulse of 25HC activates ACAT, which siphons away ER cholesterol resulting in rapid depletion of accessible cholesterol from the PM. Second, 25HC suppresses SREBP-mediated uptake and synthesis of cholesterol, resulting in sustained depletion of accessible cholesterol in the PM. We next asked whether initial ACAT activation was required for depletion of accessible cholesterol over long time periods, or whether this could be achieved simply through sustained SREBP inhibition by residual 25HC? To answer this question, we compared the responses of WT and ACAT1$^{-/-}$ cells to depletion of accessible PM cholesterol. As expected, HPCD treatment (1 hour) induced the depletion of accessible PM cholesterol in both cell lines (***Figure 4D***, *lanes 1, 2*), and this depletion was fully reversed 22 hours after HPCD removal (*lane 3*), indicating that this mode of cholesterol depletion occurred independently of ACAT activity. A different result was observed after 25HC treatment for 4 hours. In WT cells, 25HC depleted the accessible cholesterol as expected and no replenishment was observed after the 25HC was removed (***Figure 4D***, *first panel*, *lanes 4, 5*). However, in ACAT1$^{-/-}$ cells, 25HC did

not deplete accessible PM cholesterol and there was no further change after the 25HC was removed (***Figure 4D***, *third panel*, *lanes 4, 5*). Thus, without the initial action of 25HC on ACAT, the lingering intracellular 25HC that inhibits new cholesterol synthesis and uptake through suppressing SREBP activation is not enough to reduce accessible PM cholesterol, even after 22 hours.

ACAT activation by 25HC protects cells from pore formation by bacterial cytolysins

Having determined how ACAT-activating oxysterols trigger both rapid and sustained depletion of accessible cholesterol from the PM, we next sought to determine if these mechanisms are responsible for the previously reported immunological effects of 25HC. Recent studies have indicated that 25HC protects cells from pore-forming activities of bacterial cholesterol-dependent cytolysins (CDCs) that exploit accessible PM cholesterol (7, 52, 53). We used ACAT1$^{-/-}$ CHO-K1 cells as a model to test whether ACAT activation is the primary mechanism for 25HC's protection from pore formation by two CDCs, Anthrolysin O (ALO) (54, 55) and Perfringolysin O (PFO) (56, 57). Dose curve analysis showed that much lower concentrations of ALO were required to form pores in ACAT1$^{-/-}$ cells compared to WT cells (***Figure S6A***, *left panel*), consistent with the higher amounts of accessible cholesterol in the PMs of ACAT1$^{-/-}$ cells (***Figure 3B***). Moreover, stable expression of hACAT1(WT), but not inactive hACAT1(H460A), in the ACAT1$^{-/-}$ cells rendered them less susceptible to pore formation by ALO (***Figure S6A***, *right panel*). Similar results were obtained with PFO, although the extents of the dose dependency shifts were less dramatic (***Figure S6B***).

Next, we treated each of these four cell lines with 25HC for 4 hours and then measured the ability of ALO and PFO to rapidly form pores. As expected, 25HC treatment of WT cells abolished pore formation by ALO and PFO in a dose dependent manner (***Figure 5***, *first column*), consistent with 25HC's ability to deplete accessible cholesterol from the PMs of these cells (***Figure 2A***). In contrast, 25HC treatment had no effect on pore formation in ACAT1$^{-/-}$ cells (***Figure 5***, *second column*) due to its inability to deplete accessible cholesterol from the PMs of these cells (***Figure 2A***). Restoration of ACAT activity by stable expression of hACAT1(WT) reestablished the ability of 25HC to abolish pore formation, whereas inactive hACAT1(H460A) was unable to do so (***Figure 5***, *third and fourth columns*). In all four cell lines, 4HC had no effects on pore formation (***Figure 5***), consistent with this oxysterol's inability to deplete accessible cholesterol from PMs (***Figure 1D***). The above data obtained with ACAT1$^{-/-}$ CHO-K1 cells indicates that the protective effects of 25HC on macrophage lysis by CDCs primarily relies on ACAT activation.

Anti-bacterial activity of 25HC requires ACAT activation

Unlike bacterial toxins that induce rapid lysis of host cells, bacterial pathogens such as *Listeria monocytogenes* can survive for long periods of time within host cells (58, 59). We have previously shown that accessible cholesterol is required for *Listeria* to form membrane protrusions at cellular junctions and spread into neighboring cells, and that 25HC treatment for 18 hours blocks this spread (6, 60). However, given that 25HC production by immune cells can be short-lived (61, 62) and accessible cholesterol depletion by 25HC occurs rapidly (***Figure 1A***), we asked if a short pulse of 25HC could suppress long-term infection by *Listeria*. The increased accessible PM cholesterol in ACAT1$^{-/-}$ cells did not affect invasion or cell-to-cell spread of *Listeria* as similar levels of infection were observed in both WT and ACAT1$^{-/-}$ cells after 22 hours (***Figure S6C***). Moreover, infection levels were similar in the ACAT1$^{-/-}$ cells that stably expressed either hACAT1(WT) or inactive hACAT1(H460A) (***Figure S6C***). In contrast to these results, short-term incubation of WT cells with 25HC prior to infection (followed by removal of the oxysterol) reduced *Listeria* infection in a dose dependent manner (***Figure 6A***, *first column*). Strikingly, this treatment had no effect on infection of ACAT1$^{-/-}$ cells (***Figure 6A***, *second column*). The anti-bacterial activity of 25HC was restored by expression of hACAT1(WT), whereas inactive hACAT1(H460A) did not reduce infection (***Figure 6A***, *third and fourth columns*). In all four cell lines, 4HC had no effects on *Listeria* infection (***Figure 6A***), consistent with this oxysterol's inability to deplete accessible cholesterol from PMs (***Figure 1D***).

Previously, we showed that genetic ablation of cholesterol 25-hydroxylase (*Ch25h*), the enzyme that produces 25HC, in mice enhanced the transmission of *Listeria* from the gut to the spleen, and that delivery of exogenous 25HC suppressed this systemic transmission (6). To determine if the protective effects of 25HC observed in these studies were dependent on ACAT1 activation, we assessed the infectivity of ACAT1 global knock-out mice (63). To obtain robust mucosal infection, we used a murinized *Listeria monocytogenes* EGD strain carrying a mutation in Internalin A that enhances its binding affinity for mouse E-cadherin (*Lm*-InlA^{m}) (64). Consistent with our previous studies, transmission of *Lm*-InlA^{m} to liver and spleen tissues was significantly reduced in ACAT1$^{+/+}$ mice treated with 25HC (***Figure 6B****, top row*). However, 25HC was unable to protect ACAT1$^{-/-}$ mice from *Lm*-InlA^{m} infection (***Figure 6B***, *bottom row*). In contrast to what we observed in liver and spleen tissues, we observed no difference in *Lm*-InlA^{m} levels in the caecal tissues of ACAT1$^{+/+}$ and ACAT1$^{-/-}$ mice upon 25HC treatment (***Figure 6B***), indicating that 25HC protects the organism from systemic transmission and not initial bacterial invasion of the gut epithelium. These data are consistent with those obtained in cultured cells and provide evidence that 25HC elicits long-term protective effects *in vivo* through activation of ACAT.

449

450 ***25HC does not protect ACAT-deficient cells from infection by two model viruses***

451 The above studies show that ACAT activation by 25HC is a defense mechanism used by
452 cells to combat bacteria and their toxins. 25HC has also been shown to suppress highly
453 pathogenic viruses including human immunodeficiency virus (HIV), Ebola virus, Nipah virus, Rift
454 Valley fever virus, Zika virus (ZIKV), and SARS-CoV-2, the causative agent of COVID-19 (8, 65-
455 68). We asked if the anti-viral activity of 25HC was also due to the long-lasting depletion of
456 accessible PM cholesterol initiated by ACAT activation. We focused on infection by ZIKV and the
457 model human coronavirus (hCoV-OC43) in Huh7.5 cells, a human hepatoma cell line that is
458 permissive to viral infection due to defects in innate immune signaling (69, 70).

459 To test whether 25HC's antiviral effects in Huh7.5 cells were due to activation of ACAT,
460 we first needed to generate an Huh7.5 cell line that lacked ACAT activity. Unlike the CHO-K1
461 cells used above, ACAT activity in Huh7.5 cells arises from two isoforms of ACAT, ACAT1 and
462 ACAT2 (71). Therefore, we used CRISPR-Cas9 technology to disrupt both ACAT1 and ACAT2
463 genes in Huh7.5 cells, and the resulting cells were designated as Huh7.5$^{\Delta ACAT}$ cells (***Figure S7A***
464 and *Methods*). ACAT enzymatic activity, as judged by cholesteryl [^{14}C]oleate formation, was
465 stimulated by 25HC to an expected degree in Huh7.5 cells but not in Huh7.5$^{\Delta ACAT}$ cells (***Figure***
466 ***S7B***). Consistent with the diminished ACAT activity, 25HC was unable to deplete accessible
467 cholesterol from the PMs of the Huh7.5$^{\Delta ACAT}$ cells (***Figure S7C***).

468 We first compared the infection levels of ZIKV and hCoV-OC43 in Huh7.5 and Huh7.5$^{\Delta ACAT}$
469 cells after 24 hours. The ability of ZIKV to infect Huh7.5$^{\Delta ACAT}$ cells was increased by 60%
470 compared to infection of Huh7.5 cells (***Figure 7A***, *middle* and *right panels*, *gray bars*). In contrast,
471 hCoV-OC43 infection of Huh7.5$^{\Delta ACAT}$ cells was reduced by 45% compared to infection of Huh7.5
472 cells (***Figure 7B***, *middle* and *right panel*, *gray bars*). Since the relative infection levels vary in
473 opposite directions, we think it is unlikely that the differences are related to accessible PM
474 cholesterol levels in Huh7.5 and Huh7.5$^{\Delta ACAT}$ cells. We next tested the ability of 25HC to protect
475 Huh7.5 cells from these viruses. 25HC treatment for 4 hours reduced ZIKV and hCoV-OC43
476 infection by 48% and 57%, respectively (***Figure 7A*** *and* ***B***, *middle panels*, *orange bars*).
477 Strikingly, the protective effect of 25HC toward both viruses was severely attenuated in the
478 Huh7.5$^{\Delta ACAT}$ cells (***Figure 7A*** *and* ***B***, *right panel*s, *orange bars*). In all cases, treatment with 4HC
479 did not alter infection (***Figure 7A*** *and* ***B***, *blue bars*). We also noted that accessible cholesterol
480 was depleted from the PMs of Huh7.5 cells, but not Huh7.5$^{\Delta ACAT}$ cells, by 25HC treatment for 4
481 hours, and that 4HC had no effects (***Figure S7C***).

In summary, these studies demonstrate that depletion of PM accessible cholesterol through ACAT activation is a common mechanism underlying the anti-toxin, anti-bacterial, and anti-viral properties of 25HC.

Discussion

Almost 50 years ago, 25HC was identified as a potent suppressor of cholesterol synthesis (72, 73). Since then, 25HC has been found to affect virtually every aspect of cholesterol homeostasis (74). Yet, the biological role of this oxysterol has remained mysterious since mice lacking CH25H, the enzyme that produces 25HC, have no defects in cholesterol metabolism (75). A role for 25HC in the immune system was first recognized with the finding that stimulation of macrophage Toll-like receptors (TLRs) induced expression of CH25H and production of 25HC, suppressing the production of immunoglobulin A by B cells as part of the adaptive immune response (61). There is also growing evidence that 25HC exhibits potent anti-bacterial and anti-viral properties (5, 76-80), but the underlying mechanisms remain unresolved. In this study, we provide a potentially unifying model for the broad immunological activities of 25HC. The model builds on recent observations that bacteria and viruses exploit a small pool of cholesterol in the host cell's PM, termed accessible cholesterol, to promote infection (6-8). We show that 25HC manipulates pathways normally used to maintain cholesterol homeostasis to i) rapidly deplete accessible PM cholesterol; and ii) maintain this depleted state over an extended period of time to deliver long-lasting protection against bacterial and viral infection.

A striking feature of 25HC is its ability to act within 30 – 60 minutes to deplete accessible PM cholesterol (***Figure 1A***). We found that 25HC swiftly depletes accessible PM cholesterol primarily through stimulation of ACAT's enzymatic activity, and not through its effects on LXR and SREBP transcriptional pathways (***Figures 1***, ***2***). Since ACAT resides in the ER, we were surprised that its activation could rapidly deplete accessible cholesterol from the membrane of a different organelle, the PM. Our studies suggest that such depletion occurs by exploiting the rapid transport pathways that normally move cholesterol between the PM and ER to maintain an equivalence of accessible cholesterol between the two membranes (***Figure 3***). Activation of ACAT siphons off some of the ER accessible cholesterol to form cholesteryl esters, which results in an imbalance in accessible cholesterol levels between the PM and the ER. The rapid movement of cholesterol between the two membranes swiftly rectifies this imbalance and leads to a net lower level of accessible cholesterol in both membranes (***Figure 3***). Thus, 25HC exploits existing cholesterol homeostatic features to rapidly deplete accessible PM cholesterol. In line

with this model, a prescient earlier study showed that 25HC activation of ACAT in macrophages reduces a pool of PM cholesterol that is accessible for modification by the enzyme cholesterol oxidase (81).

A potentially confounding observation is that stimulation of mouse macrophage TLRs by lipopolysaccharides (LPS) increases CH25H expression only for a short period of time (~4 hours), after which CH25H expression declines down to baseline levels (61, 62). How then could short-lived production of 25HC protect cells from bacterial and viral infections that occur over much longer time periods? Remarkably, we found that in cells exposed to 25HC for short periods of time (4 hours), accessible PM cholesterol levels remained low even after 22 hours (***Figure 4A***). This result was surprising since one would expect that depletion of accessible PM cholesterol would also deplete accessible cholesterol in the ER, leading to upregulation of SREBP transcription factors that would increase cholesterol synthesis and uptake and replenish accessible PM cholesterol. Indeed, such replenishment is observed when accessible PM cholesterol is depleted by treatment with HPCD (***Figure 4B***). In contrast, after cells were exposed to 25HC for 4 hours, the residual amounts of 25HC that remained in the cells was sufficient to maintain SREBPs in their inactive state over an extended period of 22 hours (***Figure 4A***). Thus, 25HC achieves both rapid and long-lasting depletion of accessible PM cholesterol through its concerted effects on ACAT and SREBPs. Although the panel of oxysterols studied here (***Figure 1C***) is by no means an exhaustive list, it is worth noting that the four other oxysterols that deplete accessible cholesterol from PMs through stimulation of ACAT activity (20αHC, 24(*R*)HC, 24(*S*)HC, and 27HC) also suppress the activation of SREBP transcription factors (***Figure 1H***). It is attractive to speculate that these other oxysterols may also regulate accessible PM cholesterol in other biological contexts.

The model we propose for 25HC's anti-bacterial and anti-viral functions is dependent on ACAT activation as the initiator of rapid depletion of accessible PM cholesterol. In the absence of ACAT activity, 25HC loses the ability to protect cells from lysis by cytolysins secreted by *Clostridium perfringens* and *Bacillus anthracis* (***Figure 5***), infection by *Listeria monocytogenes* (***Figure 6A***), and infection by Zika virus and coronaviruses (***Figure 7***). In mammalian cells, ACAT activity arises from two isoforms – ACAT1 and ACAT2 (20). While ACAT activity can be completely abolished in cultured cells through CRISPR-mediated deletion of either or both isoforms of ACAT, an animal knockout of both isoforms of ACAT is not currently available. However, 25HC's ability to protect against infection by *Listeria monocytogenes* was completely lost in ACAT1-deficient mice (***Figure 6B***). Further studies are needed to identify the cell types

548 targeted by 25HC since the ACAT1-deficient mice lost ACAT activity in peritoneal macrophages
549 and adrenal tissue, but not in the liver (63).

550 An outstanding question that has yet to be answered is how pathogens exploit accessible
551 PM cholesterol for infection and how 25HC-mediated loss of accessible PM cholesterol provides
552 immune protection. In the case of cytolysins such as Perfringolysin O and Anthrolysin O that bind
553 accessible cholesterol on the outer PM leaflet, oligomerize, and form lytic pores, it is plausible
554 that depletion of accessible PM cholesterol would confer protection by preventing cytolysin
555 binding. However, how depletion of accessible PM cholesterol protects against intracellular
556 pathogens such as *Listeria monocytogenes* or viruses remains largely unknown. We suspect that
557 accessible PM cholesterol regulates the activities of one or more protein receptors involved in
558 these processes, as has been shown for proteins in the Hedgehog signaling pathway (82). It is
559 worth noting that cholesterol has been implicated in the regulation of several immune receptor
560 signaling complexes (83, 84). Thus, the principles and tools described in the current study
561 promise to aid in uncovering the mechanisms by which accessible PM cholesterol is exploited by
562 pathogens and is mobilized by the host immune system through 25HC and other functionally
563 related oxysterols.

564

565

566 Acknowledgements

567 We thank Francisco Bautista for his assistance during the early stages of generating ACAT-
568 deficient cells; Danya Vazquez, Bilkish Bajaj, and Chieu Nguyen for excellent technical
569 assistance; Lisa Beatty, Camille Harry, Ijeoma Dukes, and Alex Hatton for cell culture assistance;
570 and members of all our laboratories for helpful discussions. K.A.J. is the recipient of a
571 postdoctoral fellowship from the Hartwell Foundation. We are grateful for support from the
572 National Institutes of Health (AI158357 to A.R. and N.M.A., HL20948 to A.R., AI083359 to N.M.A,
573 and 5T32AI007520 to D.B.H.), the Welch Foundation (I-1731 to N.M.A., I-1793 to A.R.), and the
574 Fondation Leducq (19CVD04 to A.R.).

575

576 Author Contributions

577 D.B.H, K.A.J., M.B.O., J.G.M., J.W.S., N.M.A., and A.R. designed research; D.B.H, K.A.J.,
578 M.B.O., D.M., L.Z., M.T., C.C., M.E.A., and A.R. performed research; D.B.H, K.A.J., D.M., N.M.A.,
579 and A.R. analyzed data; D.B.H, K.A.J., N.M.A., and A.R. wrote the paper.

580

EXPERIMENTAL MODEL DETAILS

Mice

All animal experiments were performed with the approval of the Institutional Animal Care & Use Committee (IACUC) at the University of Texas Southwestern Medical Center (Approval Reference Number: APN102346). Mice were housed in 12 h light/12 h dark cycles and given ad libitum access to food and water at the UTSW Animal Resource Center. ACAT1 global knockout ($ACAT1^{-/-}$) mice were obtained from the laboratory of T.Y. Chang at Dartmouth College. To produce experimental mice, we first crossed male $ACAT1^{-/-}$ mice with WT C57BL/6J mice to generate heterozygous $ACAT1^{+/-}$ mice. $ACAT1^{+/-}$ mice were then inbred crossed to generate homozygous $ACAT1^{-/-}$ and $ACAT1^{+/+}$ mice. $ACAT1^{+/+}$ littermates were inbred crossed to generate experimental WT controls; $ACAT1^{-/-}$ mice were inbred crossed to generate experimental knock out mice. For each experiment, 9- to 14-week old mice (both sexes) were randomly assigned to each experimental group and the order of mouse dosing and sample collection were randomized between each group.

Cell Lines

All stock cultures of cells were grown in monolayer at 37°C in the indicated media (see **Reagents – *Culture Media*** in **Method Details**). CHO-K1 cells (*Cricetulus griseus*; female; ovary) were maintained in medium B in 8.8% CO_2. Scap-deficient SRD13A cells (*Cricetulus griseus*; female; ovary) (43) and Site-2 protease-deficient cells (*Cricetulus griseus*; female; ovary), in which expression of the nuclear forms of each of SREBP-1a, -1c, or -2 can be induced by muristerone A (51), were maintained in medium B supplemented with 1 mM sodium mevalonate, 20 μM sodium oleate, and 5 μg/ml cholesterol in 8.8% CO_2. HEK293A cells (human; female; kidney epithelial), LXRα/β-deficient cells (human; female; kidney epithelial) (6), HEK293T (human; female; kidney epithelial), and Huh7.5 cells (human; male; liver epithelial) were maintained in medium D in 5% CO_2. To guard against potential genomic instability, all cell lines were passaged for less than 6 weeks, after which a fresh aliquot of cells was thawed and propagated. All cell lines were confirmed to be free of mycoplasma contamination using the LookOut® Mycoplasma PCR Detection Kit (Sigma).

Bacterial Strains

For all *Listeria* infections, *Listeria monocytogenes* 10403s was grown overnight in BHI medium supplemented with 100 μg/ml streptomycin at 30°C without shaking. *Listeria monocytogenes* EGD was grown overnight BHI medium at 30°C without shaking.

Viruses

ZIKV-MR766-Venus was propagated in Huh7.5 cells as previously described (85). hCoV-OC43 was obtained from ATCC (Cat#VR-1558) and stored at -80°C until use.

METHOD DETAILS

Reagents

Buffers

Buffer A contains 50 mM Tris-HCl (pH 7.5), 150 mM NaCl, and 1 mM tris (2-carboxyethyl) phosphine (TCEP). Buffer B contains 10 mM Tris-HCl (pH 6.8), 100 mM NaCl, 1% (w/v) SDS, 1 mM EDTA, 1 mM EGTA, 20 µg/ml phenylmethylsulfonyl fluoride, and protease inhibitors (1 tablet/ 20 ml). Buffer C is PBS supplemented with 4% (v/v) paraformaldehyde. Buffer D is PBS supplemented with 2% (w/v) bovine serum albumin. Buffer E is PBS supplemented with 3% (w/v) FCS. Buffer F is PBS supplemented with 1 mM EDTA. Buffer G is Hank's Balanced Salt Solution (HBSS) supplemented with 10% (v/v) FCS.

Culture Media

Medium A is a 1:1 mixture of Ham's F-12 and Dulbecco's modified Eagle's medium (DMEM) supplemented with 100 units/ml penicillin and 100 µg/mL streptomycin sulfate. Medium B is medium A supplemented with 5% (v/v) FCS. Medium C is medium A supplemented with 5% (v/v) LPDS, 50 µM sodium compactin, and 50 µM sodium mevalonate. Medium D is DMEM (high glucose) supplemented with 5% (v/v) FCS, 100 units/ml penicillin, and 100 µg/mL of streptomycin sulfate. Medium E is DMEM (high glucose) supplemented with 10% (v/v) FCS and 1X MEM non-essential amino acids (NEAA). Medium F is medium E supplemented with 100 units/ml penicillin and 100 µg/mL streptomycin sulfate. Medium G is DMEM (high glucose) supplemented with 3% (v/v) FCS and 1X NEAA. Medium H is medium A supplemented with 1X NEAA, 20 mM Hepes (pH 7.4), and 4 µg/ml hexadimethrine bromide. Medium I is medium B without penicillin or streptomycin sulfate.

ACAT-deficient cell lines

Mammalian cells express two isoforms of ACAT, ACAT1 (also designated as SOAT1) and ACAT2 (also designated as SOAT2), both of which convert cholesterol to cholesteryl esters. Previous studies have shown that ~99% of ACAT activity in CHO cells arises from ACAT1 (40, 41), whereas ACAT activity in Huh7.5 cells arises from both ACAT1 and ACAT2 (71). To generate

cells that lacked ACAT activity, we therefore disrupted the ACAT1 gene in CHO-K1 cells and both the ACAT1 and ACAT2 genes in Huh7.5 cells using CRISPR-Cas9 technology (86).

To generate mutant CHO-K1 cells, guide RNAs targeting exons 2 (5'-AGGAACCGGCTGTCAAAATC-3') and 14 (5'-ATAGCTCAAGCAGACAGCGA-3') of ACAT1 (***Figure S3A***) were designed using the Benchling CRISPR guide RNA design tool (https://www.benchling.com/crispr) and cloned into the lentiviral vector lentiCRISPR v2 (Addgene 52961) (87). For lentivirus production, HEK293T cells were set up in medium E at a density of 4 x 10^5 cells per well of polylysine-coated 6-well plates. The next day, cells were transfected with four plasmids: i) a puromycin-selectable lentiCRISPR v2 plasmid encoding a guide targeting exon 2 of ACAT1 (0.5 µg); ii) a blasticidin-selectable lentiCRISPR v2 plasmid encoding a guide targeting exon 14 of ACAT1 (0.5 µg); iii) a plasmid encoding HIV gag-polymerase (0.8 µg); and iv) a plasmid encoding vesicular stomatitis virus glycoprotein (0.2 µg). Transfections were carried out in 1 ml of medium G using X-tremeGENE 9 according to the manufacturer's protocol. After 6 h, the media containing transfection reagents was removed and replaced with 1.5 ml of fresh medium G. After 48 h, the media was removed and stored, and 1.5 ml of fresh medium G was added to the cells. After an additional 24 h, media was removed and combined with the media collected after 48 h. The pooled media was supplemented with 20 mM Hepes-NaOH (pH 7.4) and 4 µg/ml hexadimethrine bromide, a cationic polymer that increases the efficiency of lentiviral transduction, and subjected to centrifugation at 800 x g for 5 min. The supernatants containing lentiviral particle-rich media were stored at -80°C.

To generate ACAT1-deficient cells using this lentivirus, CHO-K1 cells were set up on day 0 in medium B at a density of 1 x 10^5 cells per well of a 12-well plate. On day 1, media was removed and replaced with 1 ml medium H plus 120 µl of lentiviral particle-rich medium. The plate was then subjected to centrifugation at 1000 x g for 30 min at 37°C, following which the spin-inoculated cells were placed in a 37°C incubator with 5% CO_2. After 24 h, the media was removed, cells were washed twice with PBS, following which 1 ml of medium B was added to each well. After 72 h, transduced cells were selected by virtue of their ability to survive after incubation in medium B supplemented with 6 µg/ml puromycin and 12 µg/ml blasticidin for 14 days. During the 14-day selection period, media was removed every 2-3 days and replaced with fresh medium B supplemented with 6 µg/ml puromycin and 12 µg/ml blasticidin. Single cells were isolated by FACS and used to establish clonal cell lines. The ACAT1 genes in these lines were analyzed by genomic sequencing using primers to amplify exon 2 (5'-CTACAAGAGCTAGTTTCAGG-3' and 5'-CCCTGTGTGTACAGTGCCTT-3') and exon 14 (5'-

TCACTCACCTTGAAGACCCA-3' and 5'-GGGTTCCTCTCTACACACTCA-3'). Sequencing analysis revealed one cell line that had a 4 bp deletion in both alleles of exon 14 resulting in a premature stop codon (***Figure S3A***). We did not detect any disruptions in the sequence of exon 2. This cell line was designated as CHO-K1 ACAT1$^{-/-}$ and used for analysis of the role of ACAT1 in maintaining accessible cholesterol on PMs.

The CHO-K1 ACAT1$^{-/-}$ cell line was also used as template to generate two additional cell lines expressing either WT human ACAT1 or a mutant version of human ACAT1 where H460, the catalytic histidine residue, was mutated to alanine (H460A). To achieve this goal, we used Gateway cloning methods to introduce either the WT or mutant ACAT1 gene into the pTRIP.CMV.IVSB.ires.TagRFP destination lentiviral vector (88). The ACAT1 genes were inserted upstream of two elements in the pTrip vector, an internal ribosomal entry site and Tag-RFP. Lentiviral particle-rich media was generated as described above and used to transduce the CHO-K1 ACAT1$^{-/-}$ cells using similar procedures as described above for CHO-K1 cells. After 72 h, the transduced cells were washed once with PBS, removed from each well of 12-well plates by trypsinization, and transferred to 10-cm dishes in medium B. This procedure was repeated until a total of 2 x 10^7 cells were obtained. These cells were sorted by FACS to select RFP-positive cells from which clonal cell lines were established. Two cell lines that showed robust expression of human ACAT1 (WT or H460A versions) were selected for the studies reported here. All CHO-K1 ACAT1$^{-/-}$ cells were maintained under identical culture conditions as the parental CHO-K1 cells.

To generate an ACAT-deficient Huh7.5 cell line, we used CRISPR/Cas technology to first delete ACAT1 in Huh7.5 cells and then deleted ACAT2 in these ACAT1-deficient cells. Guide RNAs targeting exon 6 in human ACAT1 (5'-CACCAGGTCCAAACAACGGT-3') or exon 2 in human ACAT2 (5'-GGTCCATTGTACCAAGTCCG-3') (***Figure S7A***) were designed using CHOP-CHOP (https://chopchop.cbu.uib.no/). These guide RNAs were cloned into either a puromycin-selectable (exon 6 of ACAT1) or a blasticidin-selectable (exon 2 of ACAT2) lentiviral vector lentiCRISPR v2, and lentiviruses were generated as described above.

To generate ACAT-deficient cells using these lentiviruses, Huh7.5 cells were set up on day 0 in medium E at a density of 7 x 10^4 cells per well of a 12-well plate. On day 1, media was removed and replaced with 0.4 ml medium G plus 0.1 ml of lentivirus targeting exon 6 of ACAT1. After 6 h, 2 mL of medium F was added to each well without removing the lentivirus. After additional incubation for 72 h, cells from 3 wells of the 12-well plate were collected by

trypsinization and set up in a single well of a 6-well plate. After 24 h, the media was removed, cells were washed twice with PBS, and 2 ml of medium F supplemented with 8 µg/ml puromycin was added to each well. Puromycin selection was carried out for 14 days. During this selection period, media was removed every 2-3 days and replaced with 2 ml of fresh medium F supplemented with 8 µg/ml puromycin. After selection, single cells were isolated by FACS and set up in 96-well plates in 100 µl of medium F. Unfortunately, we were unable to establish clonal cell lines from these single-cell clones. To overcome this problem, 24 h after the isolated single cells were set up in 96-well plates, we added Huh7.5 cells (1.5×10^3) in 100 µl of medium F supplemented with additional FCS to reach a final concentration of 40% (v/v). After 5 days, 100 µl of medium F without FCS was added to each well to replenish media lost to evaporation. This replenishment step was repeated on the 10^{th} day. After 15 days, the media was removed and replaced with 200 µl of medium F supplemented with 8 µg/ml puromycin. After an additional 7 days, only lentiviral-transduced cells survived, and these cells were collected by trypsinization and set up in 24-well plates in medium F supplemented with 8 µg/ml puromycin. After further selection for 3 days, surviving cells were expanded in medium F to obtain enough cells for genomic sequencing. The ACAT1 genes were analyzed using primers to amplify exon 6 (5'-CAGCGTATTAACGTTGTGGTGT-3' and 5'-GCCCAATGTTGAAACAGAAAAT-3'). Sequencing analysis of ACAT1 revealed one cell line that had a 1 bp insertion in one allele and a 63 bp deletion in the other allele, resulting in premature stop codons in both cases (***Figure S7A***). This ACAT1-deficient cell line was transduced as described above with a lentivirus targeting exon 2 of ACAT2. Selection was carried out as described above, except that medium F supplemented with 6 µg/ml blasticidin was used in all selection steps. Candidate cell lines were analyzed by genomic sequencing using primers to amplify exon 2 of ACAT2 (5'-CAACTTCCCCTTCTAGTAGCCC-3' and 5'-CTTTATCACCAAGCCTCACTCC-3'). Sequencing analysis of ACAT2 revealed one cell line that had a 7 bp deletion in one allele and a 1 bp insertion in the other allele, resulting in premature stop codons in both cases (***Figure S7A***). This cell line, designated as Huh7.5$^{\Delta ACAT}$, was maintained under identical culture conditions as the parental Huh7.5 cells and used for further studies involving viral infections.

Protein purification and labeling

Recombinant His_6-FLAG-ALOD4 and His_6-Neon-FLAG-ALOD4 (designated as fALOD4-Neon) were purified by nickel chromatography followed by gel filtration chromatography as described previously (89). In some cases, the lone engineered cysteine on purified His_6-FLAG-ALOD4 was labeled with fluorescein-5-maleimide as described previously for other maleimide

743 dyes (90) and the fluorescent protein was designated as fALOD4-fluorescein. Recombinant OlyA-
744 His_6 was purified by nickel chromatography followed by gel filtration chromatography as described
745 previously (29). In some cases, the lone engineered cysteine on purified OlyA-His_6 was labeled
746 with either Alexa Fluor 647 C_2-maleimide or fluorescein-5-maleimide as described previously (29),
747 and the fluorescent proteins were designated as fOlyA-647 or fOlyA-fluorescein, respectively.
748 Recombinant His_6-tagged versions of full-length (FL) ALO and PFO were purified by nickel
749 chromatography followed by gel filtration as described previously (28). fALOD4-Neon and fOlyA-
750 647, in buffer A supplemented with 20% (v/v) glycerol, were flash frozen in liquid N_2 and stored at
751 -80°C for up to six months. The fluorescein-labeled proteins were stored in buffer A at 4°C and
752 used within two weeks. His_6-FLAG-ALOD4, His_6-ALO(FL), His_6-PFO(FL), and OlyA-His_6 were
753 stored in buffer A at 4°C and used within one month.

754 ## Assays

755 ### *Immunoblot analysis*

756 After indicated treatments, cells were harvested as described previously (30). The
757 following primary antibodies were used: anti-His (1:1,000 dilution) to detect His_6-FLAG-ALOD4
758 and OlyA-His_6, anti-β actin (1:1,000 dilution) to detect actin, anti-ACAT1 (1:1,000 dilution) to
759 detect ACAT1, IgG-7D4 (10 μg/mL) to detect SREBP2, and anti-FLAG (1:1,000 dilution) to detect
760 muristerone-induced nuclear forms of SREBPs. Bound antibodies were visualized using a
761 1:5,000 dilution of either donkey anti-mouse IgG (Jackson ImmunoResearch) or goat anti-rabbit
762 IgG (Jackson ImmunoResearch) conjugated to horseradish peroxidase. Membranes were
763 exposed to either Phoenix Blue X-Ray film (Phoenix Research Products) or UltraCruz
764 Autoradiography (Santa Cruz Biotechnology) at room temperature for 1-120 s for all cases.

765 ### *Cell surface binding of ALOD4 or OlyA after treatment with oxysterols*

766 On day 0, cells were set up as indicated in the Figure Legends. On day 1, media was
767 removed, cells were washed twice with PBS, then treated with media containing the indicated
768 concentration of oxysterols solubilized in ethanol. In each experiment, the amount of ethanol
769 added to each well was held constant (maximum 0.2%). After incubation for the indicated times,
770 media was removed and replaced with media supplemented with 3 μM of either His_6-Flag-ALOD4
771 or OlyA-His_6. After incubation for 30 min at 37°C, cells were washed twice with PBS, harvested
772 in buffer B, and equal aliquots were subjected to immunoblot analysis using anti-His and anti-
773 actin antibodies. In some cases, the immunoblot signals were quantified by densitometry analysis
774 using ImageJ as follows. In each experiment (dose curve or time curve), the anti-actin and anti-

His immunoblot signals for each condition were quantified. The actin signal for each condition was divided by the highest value for the actin immunoblot signal in that experiment to generate relative values for actin signal. Next, the His immunoblot signal for each condition was divided by the relative actin signal for that condition to generate a normalized His signal for each condition. The normalized His signal at the zero-timepoint or zero-concentration was set to 100% and all other values were reported relative to this value. Further details can be found in the Figure Legends.

Microscopy

Cells were treated with oxysterols and fluorescent sensor proteins as indicated in Figure Legends. Oxysterols were solubilized in ethanol and the amount of ethanol added during each treatment was held constant (maximum 0.2%). After treatment, cells were washed twice with PBS and then fixed with 500 µl of buffer C. After incubation at room temperature (RT) for 15 min, cells were washed 4 times with PBS and then treated with 500 µl of buffer D. After incubation on an orbital shaker at RT for 30 min, buffer D was removed and replaced with 500 µl of buffer D supplemented with 1 µg/ml DAPI. After further incubation on an orbital shaker at RT for 30 min, cells were washed twice with PBS and either imaged immediately or post-fixed with 500 µl buffer C and imaged at a later time. Images were acquired on a Nikon Eclipse *Ti* epifluorescence microscope with a 60x objective.

Measuring ALOD4 and OlyA binding to cells by flow cytometry

Cells were set up in 24-well plates on day 0 and subjected to treatments as indicated in the Figure Legends. On day 2, after incubation with fluorescent sensor proteins at 37°C for 30 min, media was removed, cells were washed twice with 500 µl of PBS followed by addition of 100 µl of Accumax. After incubation at 37°C for 5 min, detached cells were transferred to a 96-well plate where each well contained 100 µl of PBS supplemented with 2% (v/v) PFA. After incubation on ice for 20 min, cells were subjected to centrifugation at 1,000 x g for 5 min at RT. The supernatant was removed and the cell pellets were resuspended in 150 µl of buffer E and subjected to FACS analysis using a Stratedigm S100 EX Flow Cytometer. Data was analyzed using FlowJo software version 10.

Quantification of intracellular levels of 25HC

Cells were set up in 24-well plates on day 0 and subjected to treatments as indicated in the Figure Legends. Mass spectrometry analysis of the cellular content of 25HC was performed

806 as described previously (91). Briefly, lipids were extracted from cellular fractions using a modified
807 Bligh and Dyer extraction procedure with a 1:1:1 mixture of methanol, dichloromethane, and PBS.
808 The organic extracts were saponified to generate a pool of free oxysterols, which were further
809 purified using solid-phase extraction. Samples were evaporated under a gentle stream of nitrogen
810 and reconstituted in 90% methanol. 25HC levels were measured with isotope dilution mass
811 spectrometry using a deuterated analog of 25-hydroxycholesterol (d6) added to the sample prior
812 to extraction as a standard for quantification. Lipid extracts were resolved and detected using
813 high performance liquid chromatography (HPLC) coupled to a triple quadrupole mass
814 spectrometer (MS) through an electrospray ionization interface. The content of 25HC in whole
815 cells is expressed relative to the protein content in those same cells as determined with a BCA
816 protein assay kit.

817 ***Cholesterol esterification***

818 Incorporation of [^{14}C] oleate into cholesteryl [^{14}C] oleate in cultured cells after oxysterol
819 addition was determined using previously described methods (33).

820 ***Measuring ALOD4 binding to red blood cells***

821 Red blood cells (RBCs) were isolated from rabbit whole blood (Innovative Research; Novi,
822 MI) using a previously described procedure (31). Briefly, rabbit whole blood was subjected to
823 centrifugation at 200 x *g* for 10 min at 4°C. The supernatant was removed, and the cell pellet was
824 resuspended in an equal volume of ice-cold Buffer F and then subjected to centrifugation at 500
825 x g for 10 min at 4°C. The supernatant was removed, and the cell pellet was resuspended in an
826 equal volume of ice-cold Buffer F and then subjected to centrifugation at 1000 x g for 20 min at
827 4°C. After removing the supernatant, the cell pellet was resuspended in 9 volumes of Buffer F
828 and stored at 4°C for up to 7 days.

829 For each binding assay, RBCs (500 µl) were incubated without or with 5 µM of the
830 indicated oxysterols for 4 h, or 1% (w/v) HPCD at RT for 1 h. As controls for hemolysis, RBCs
831 (500 µl) were incubated with 1% (v/v) Triton-X100 for 4 h. After incubations, aliquots of the binding
832 assays were transferred to new tubes. One aliquot (200 µl) was transferred to a tube containing
833 5 µl of a stock solution of fALOD4-Neon (final concentration of 1 µM) and incubated at RT for 30
834 min. A portion of this mixture (150 µl) was then transferred to a 96-well plate and fALOD4-Neon
835 binding was measured by analyzing 10,000 RBCs for each condition on a Stratedigm S1000 EX
836 Flow Cytometer (BD Biosciences). Fluorescently labeled RBCs were analyzed using FlowJo

software version 10 (Ashland, OR) and geometric mean fluorescent intensity (gMFI) of each population was calculated to quantify fALOD4-Neon binding. The other aliquot (250 µl) was subjected to centrifugation (350 x g for 15 min at 20°C) and a portion of the supernatant (125 µl) was transferred to 96-well plates. The absorbance at 540 nm was measured using a microplate reader (FLUOstar Optima) to assess hemoglobin release from lysed red blood cells. In all treatments, hemolysis was less than 10%.

Measuring pore formation by full-length PFO or ALO

To measure the dose dependence for pore formation by PFO and ALO, cells were set up in 48-well plates on day 0 as indicated in the Figure Legends. On day 1, media was removed, cells were washed twice with HBSS, followed by addition of HBSS containing either His_6-PFO(FL) or His_6-ALO(FL). After incubation for 15 min at 37°C, media was removed, cells were washed once with HBSS, then treated for 10 min at RT in the dark (wrapped in aluminum foil) with 100 µl of HBSS supplemented with Ghost Dye™ Violet 450 (1:1000), a dye that labels primary amines and is commonly used to assess membrane integrity. The labeling reaction was quenched by addition of 500 µl of buffer G for 2 min, after which the media was removed and replaced with 100 µl of Accumax, following which detached cells were transferred to a 96-well plate where each well contained 100 µl of HBSS supplemented with 2% (v/v) PFA. After incubation for 20 min at 4°C, cells were subjected to centrifugation at 800 x g for 5 min at 20°C. The supernatant was removed and the cell pellets were resuspended in 150 µl of buffer E and subjected to FACS analysis using a Stratedigm S100 EX Flow Cytometer. Data was analyzed using FlowJo software version 10. Pore formation was assessed as the percentage of cells that were labeled by Ghost Dye™ Violet 450. The highest percentage value for each cell line treated with either His_6-PFO(FL) or His_6-ALO(FL) was set to 100, and all other values for that cell line were normalized to this set-point.

To assess the effects of oxysterols on pore formation, cells were set up in 48-well plates on day 0 as indicated in the Figure Legends. On day 1, media was removed and replaced with medium B supplemented with varying concentrations of the indicated oxysterol. After incubation for 4 h at 37°C, media was removed, cells were washed twice with 500 µl of HBSS, followed by addition of HBSS containing either 100 pM of His_6-PFO(FL) or 500 pM of His_6-ALO(FL). Pore formation was assessed as described above. The percentage of cells with pore formation in the absence of oxysterol treatment was set to 100% for each replicate, and all other values were normalized to this set-point.

Inhibition of Listeria monocytogenes infection by oxysterols in cultured cells

All cell culture steps were carried out in an incubator at 37°C and 5% CO_2. On day 0, the indicated CHO-K1 cell lines were set up in Medium I at a density of 1 x 10^5 cells per well of a 24-well plate. Also on day 0, a glycerol stock of *Listeria monocytogenes* strain 10403s expressing green fluorescent protein (GFP; kindly provided by D. Portnoy, UC Berkeley) was used to inoculate 3 ml of brain heart infusion (BHI) medium supplemented with 100 µg/ml streptomycin. After incubation for 16 – 18 h at 30°C without shaking, 1 ml of the *Listeria* culture was subjected to centrifugation at 16,000 x g for 1 min at RT. The cell pellet was resuspended in 1 ml of PBS and the centrifugation step was repeated. The resulting cell pellet was resuspended in 1 ml of PBS and the optical density at 600 nm (OD_{600}) was measured. Also on day 1, media for the CHO-K1 cells was supplemented with the indicated concentrations of oxysterols. After 4 h, the cells were infected with the *Listeria* in PBS at a multiplicity of infection (MOI) of 1 for 90 min. Cells were then washed twice with 1 ml of PBS that had been pre-warmed to 37°C, followed by addition of 1 ml of Medium I supplemented with 50 µg/ml of gentamicin to kill extracellular bacteria and prevent new infections. After 20 h at 37°C, media was removed, cells were washed twice with 1 ml of PBS, and harvested with 500 µl of PBS containing 0.5% (v/v) Triton X-100. To determine the extent of infection, cell lysates were serial diluted in PBS, plated on BHI agar supplemented with 100 µg/ml streptomycin, and incubated overnight at 37°C. The next day, colonies on each plate were counted. The value for the level of infection in the absence of oxysterols was set to 100% for each replicate, and all other values were normalized to this set-point.

Inhibition of L. monocytogenes infection in a mouse model

We obtained homozygous ACAT1$^{-/-}$ global knockout mice (63) from Dr. T.Y. Chang (Dartmouth College). On days 1 – 7, 9- to 14-week-old wild type C57BL/6J and ACAT1$^{-/-}$ mice were injected once daily intraperitoneally with either 25HC (5 mg/kg in 10% ethanol) or vehicle (10% ethanol). On day 3, a glycerol stock of *Listeria monocytogenes* strain EGD harboring a mutation in Internalin A that enhances its binding affinity for murine E-cadherin (*Lm*-InlA^m) (64) was used to inoculate 30 ml of BHI medium. After incubation for 16-18 h at 30°C without shaking, the media containing *Lm*-InlA^m was subjected to centrifugation at 4,000 x g for 20 min at 4°C. The cell pellet was resuspended in 30 ml of PBS and the centrifugation step was repeated. The resulting cell pellet was resuspended in 20 ml of PBS and the OD_{600} was measured to quantify *Lm*-InlA^m. An aliquot corresponding to 10^9 *Lm*-InlA^m/mouse was subjected to centrifugation at 4,000 x g for 15 min at 4°C, and the cell pellet was resuspended in a mixture of PBS and 50 mg/ml $CaCO_3$ (final ratio of 2:3, respectively). On day 4, the mice were orally infected with 1 x 10^9 *Lm*-InlA^m intragastric gavage prior to being injected intraperitoneally with 25HC. On day 7, 4 h after

902 25HC injection, the spleen, liver, and caecum tissues of each mouse was collected. The spleens
903 and livers were homogenized in 2 ml of PBS, and serial dilutions of the homogenates were plated
904 on BHI agar plates to quantify *Lm*-InlA^{m}. Caecum tissues were removed, longitudinally dissected,
905 and caecum content was lightly scraped, followed by three sequential washes in 2 ml of PBS.
906 Tissues were shaken in 4 ml of RPMI-1640 supplemented with 100 μg/ml of gentamicin at RT.
907 After 30 min, tissues were vortexed for 5 sec. After an additional 30 min of shaking at RT, 10 ml
908 of PBS was added and tissues were subjected to centrifugation at 3,000 x g for 5 min at 4°C. The
909 supernatant was removed, replaced with 5 ml of PBS and the centrifugation step was repeated.
910 The supernatant was removed and replaced with 2 ml of PBS. Following homogenization of the
911 tissues, serial dilutions of the homogenates were plated on BHI agar plates to quantify *Lm*-InlA^{m}.

912 ***Inhibition of viral infections by oxysterols***

913 All cell culture steps were carried out in an incubator with 5% CO_2 at the indicated
914 temperatures. On day 0, Huh7.5 or Huh7.5$^{\Delta ACAT}$ cells were set up in medium F at a density of 8
915 x 10^4 cells per well of a 24-well plate. On day 1, the media was removed and replaced with 1 ml
916 of medium F supplemented with 5 μM of the indicated oxysterol. After 4 h at 37°C, the media
917 was removed and replaced with 200 μl of either hCoV-OC43 virus or ZIKV-MR766-Venus virus
918 in OptiMEM and incubated at 33°C or 37°C, respectively. After 1 h, 800 μl of medium F was
919 added to each well and maintained at either 33°C or 37°C as indicated above. After 24 h, cells
920 were harvested with Accumax, mixed with a 4% (v/v) stock solution of PFA in PBS (1% final
921 concentration), and incubated for 10 min at RT, following which cells were analyzed by FACS
922 either immediately or stored at 4°C and processed at a later time.

923 Zika-infected cells were subjected to centrifugation at 1,500 x g for 5 min at RT. The
924 supernatants were removed, and the cell pellets were resuspended in 150 μl of buffer E prior to
925 FACS analysis.

926 OC43-infected cells were subjected to centrifugation at 1,500 x g for 5 min at RT. The
927 supernatants were removed, and the cell pellets were resuspended in 50 μl of BD
928 Cytofix/Cytoperm Solution. After incubation for 20 min at RT, 150 μl of BD Wash/Perm Solution
929 was added to each sample, after which samples were subjected to centrifugation at 1,500 x g for
930 5 min at RT. The supernatant was removed, and cell pellets were resuspended in 200 μl of BD
931 Wash/Perm Solution, and subjected to centrifugation at 1,500 x g for 5 min at RT. After removing
932 the supernatant, cell pellets were resuspended in 50 μl of anti-coronavirus group antigen antibody
933 (1:50). After incubation for 30 min at RT, 150 μl of BD Wash/Perm Solution was added, and

934 samples were subjected to centrifugation at 1,500 x g for 5 min at RT. The supernatant was
935 removed, and cell pellets were resuspended in 200 µl of BD Wash/Perm Solution and subjected
936 to centrifugation at 1,500 x g for 5 min at RT. The supernatant was removed, and cell pellets were
937 resuspended in 50 µl of Goat anti-mouse AlexaFluor488 (1:1000). After incubation in the dark
938 (wrapped in aluminum foil) for 30 min at RT, 150 µl of BD Wash/Perm Solution was added and
939 samples were subjected to centrifugation at 1,500 x g for 5 min at RT. The supernatant was
940 removed, and cells were resuspended in 200 µl of BD Wash/Perm Solution and subjected to
941 centrifugation at 1,500 x g for 5 min at RT. After this final step, the supernatant was removed,
942 and cells were resuspended in 150 µl of buffer E and analyzed on a Stratedigm S1000 EX Flow
943 Cytometer using the GFP channel. Infection levels were determined as the percentage of Venus-
944 positive cells (indicating Zika infection) or AlexaFluor488-positive cells (indicating OC43 infection)
945 from at least 7,500 single cells per replicate, as assessed by FlowJo software.

946 ## QUANTIFICATION AND STATISTICAL ANALYSIS

947 All experiments were conducted at least three times with different litters of mice and with different
948 batches of cells set up on different days. Data are shown as the mean +/- standard error of
949 measurement (SEM), unless otherwise stated. Statistical significance was calculated using
950 GraphPad Prism and is indicated in the figures according to the following key: non-significant (ns)
951 $p>0.05$; * $p\leq0.05$; ** $p\leq0.01$; and *** $p\leq0.001$.

952 ## MATERIALS AVAILABILITY

953 All reagents generated in this study are available from the authors with a completed Materials
954 Transfer Agreement.

955

956 ## TABLE OF REAGENTS

REAGENT or RESOURCE	SOURCE	IDENTIFIER
Antibodies		
Donkey Polyclonal Peroxidase-AffiniPure Anti-Mouse IgG (H+L)	Jackson ImmunoResearch	Cat#715-035-150; RRID: AB_2340770
Goat Polyclonal Peroxidase AffiniPure Anti-Rabbit IgG (H+L)	Jackson ImmunoResearch	Cat#111-035-003; RRID: AB_2313567
Mouse Monoclonal Anti-Coronavirus Group Antigen, nucleoprotein of OC-43, 229E strain, clone 542-7D	Millipore Sigma	Cat# MAB9013; RRID:AB_95425
Mouse Monoclonal Anti-FLAG M2 clone	Sigma-Aldrich	F1804; RRID: AB_262044
Mouse Monoclonal Anti-His Tag, clone HIS.H8	Millipore	Cat#05-949; RRID: AB_492660
Mouse Monoclonal Anti-SREBP2	Ref. (92)	IgG-7D4

Mouse Polyclonal Goat anti-Mouse IgG (H+L) Cross-Adsorbed Secondary Antibody, Alexa Fluor 488	Thermo Fisher Scientific	Cat#A-11001; RRID:AB_2534069
Rabbit Polyclonal Anti-ACAT1	Novus	Cat#NB400-141; RRID: AB_10001588
Bacterial and virus strains		
BL21 (DE3) pLysS *Escherichia coli* competent cells	Invitrogen	Cat#C606003
hCoV-OC43	ATCC	VR-1558
Listeria monocytogenes 10403s	Ref. (93)	Gift from Dr. Daniel Portnoy, University of California, Berkeley
Listeria monocytogenes EGD $InlA^{mut}$	(64)	Gift from Dr. Wolf-Dieter Schubert, University of Pretoria, South Africa
Chemicals, peptides, and recombinant proteins		
19-hydroxycholesterol	Steraloids	Cat#C6470-000
2-Hydroxypropyl-b-cyclodextrin (HPCD)	Cyclodextrin Technologies Development	Cat#THPB-P
20α-hydroxycholesterol	Avanti Polar Lipids	Cat#700156
22(*R*)-hydroxycholesterol	Avanti Polar Lipids	Cat#700058
22(*S*)-hydroxycholesterol	Avanti Polar Lipids	Cat#700057
24(*R*)-hydroxycholesterol	Avanti Polar Lipids	Cat#700071
24(*S*)-hydroxycholesterol	Avanti Polar Lipids	Cat#700061
25-hydroxycholesterol	Avanti Polar Lipids	Cat#700019
25-hydroxycholesterol-3-sulfate	Avanti Polar Lipids	Cat#700017
25-hydroxycholesterol-d6	Avanti Polar Lipids	Cat#700053
27-hydroxycholesterol	Avanti Polar Lipids	Cat#700021
4',6-Diamidino-2-phenylindole dihydrochloride	Millipore Sigma	Cat#D8417
4β-hydroxycholesterol	Avanti Polar Lipids	Cat#700036
7α-hydroxycholesterol	Avanti Polar Lipids	Cat#700034
Accumax	Innovative Cell Technologies	Cat#AM105
Alexa Fluor 647 C_2-maleimide	Thermo Fisher Scientific	Cat#A20347
Blasticidin S HCl	Thermo Fisher Scientific	Cat#A1113903
Bovine serum albumin	Millipore Sigma	Cat#P0834
Brain Heart Infusion Agar	Thermo Fisher Scientific	Cat#DF0418
Brain Heart Infusion Broth	Thermo Fisher Scientific	Cat#DF0037
Cholesterol	Millipore Sigma	Cat#C8667
cOmplete™, EDTA-free Protease Inhibitor Cocktail	Roche	Cat# 05056489001
Dulbecco's Modified Eagle Medium (DMEM) – high glucose	Sigma	Cat#D6429
Dulbecco's Modified Eagle Medium (DMEM) – low glucose	Sigma	Cat#D6046
Dulbecco's Modified Eagle Medium (DMEM)/F-12 (1:1 mixture)	Corning	Cat#10-090-CV
Dulbecco's phosphate buffered saline (PBS)	Thermo Fisher Scientific	Cat#MT21031CV
Fetal Calf Serum	Sigma-Aldrich	Cat#F2442

Fluorescein-5-maleimide	Thermo Fisher Scientific	Cat#62245
Gentamicin	Quality Biological	Cat#120-098-661
Ghost Dye™ Violet 450	Tonbo biosciences	Cat#13-0863
Hanks Balanced Salt Solution (HBSS)	Millipore Sigma	Cat#14175-095
Hexadimethrine bromide	Thermo Fisher Scientific	Cat#107689
MEM Non-Essential Amino Acids Solution (100X)	Thermo Fisher Scientific	Cat#11140050
Methyl-β-cyclodextrin, randomly methylated (MCD)	Cyclodextrin Technologies Development	Cat#TRMB-P
Muristerone A	Sigma-Aldrich	Cat#M7888
Opti-MEM	Thermo Fisher Scientific	Cat#31985062
Paraformaldehyde	Alfa Aesar	Cat#43368
Penicillin/Streptomycin	Gibco	Cat#15140-122
Phenylmethylsulfonyl fluoride (PMSF)	Goldbio	Cat#P-470-25
Puromycin	Thermo Fisher Scientific	Cat#A1113803
Rabbit Whole Blood	Innovative Research	Cat#IGRBWBK2E10ML
Sodium compactin	(50)	N/A
Sodium mevalonate	(50)	N/A
Tris (2-carboxyethyl) phosphine Hydrochloride	Goldbio	Cat#TCEP1
Critical commercial assays		
Cytofix/Cytoperm Fixation/Permeabilization Kit	BD Biosciences	Cat#554714; RRID: AB_2869008
LookOut® Mycoplasma PCR Detection Kit	Millipore Sigma	Cat# MP0035
Microplate BCA Protein Assay Kit	Thermo Fisher Scientific	Cat#23252
Experimental models: Cell lines		
Hamster: CHO-K1	ATCC	CCL-61
Hamster: CHO-K1 ACAT1$^{-/-}$	This paper	N/A
Hamster: CHO-K1 ACAT1$^{-/-}$; hACAT1(WT)	This paper	N/A
Hamster: CHO-K1 ACAT1$^{-/-}$; hACAT1(H460A)	This paper	N/A
Hamster: M19 (stable derivatives that express truncated dominant-positive forms of SREBP-1a, -1c, and -2)	(51)	N/A
Hamster: SRD13A	(43)	N/A
Human: HEK293T	(88)	N/A
Human: HEK293A	(6)	N/A
Human: HEK293A LXRα/β-deficient cells	(6)	N/A
Human: Huh7.5	(88)	N/A
Human: Huh7.5$^{\Delta ACAT}$	This paper	N/A
Experimental models: Organisms/strains		
Mouse: C57BL/6J: Wild type	The Jackson Laboratory	Cat#000664
Mouse: ACAT1$^{+/+}$: C57BL/6J$^{ACAT1+/+}$	This paper	N/A
Mouse: ACAT1$^{-/-}$: C57BL/6J$^{ACAT1-/-}$	(63)	Gift from Dr. T.Y. Chang, Dartmouth College

Oligonucleotides		
Guide RNA sequence targeted for CRISPR/Cas9 editing are listed in Table S1	This paper	N/A
Primers for confirmation of CRISPR/Cas9 editing are listed in Table S2	This paper	N/A
Recombinant DNA		
pCDNA6.ZikaMR766.Venus3115Intron HDVr	(85)	N/A
pGag-Pol	Gift from Dr. Charles Rice, Rockefeller University	N/A
pLentiCRISPRv2-Blast	Addgene	Cat#98293
plentiCRISPRv2-Puro	Addgene	Cat#98290
pRSET-B ALO FL	(28)	N/A
pRSET-B His_6-FLAG-ALOD4	(89)	N/A
pRSET-B His_6-Neon-FLAG-ALOD4	(89)	N/A
pRSET-B OlyA-His_6	(89)	N/A
pRSET-B PFO FL	(28)	N/A
pTRIP.CMV.hACAT1.ires.TagRFP	This paper	N/A
pTRIP.CMV.hACAT1(H460A).ires.TagRFP	This paper	N/A
pTRIP.CMV.IVSB.ires.TagRFP	(88)	N/A
pVSV-Glyoprotein	Gift from Dr. Charles Rice, Rockefeller University	N/A
Software and algorithms		
Benchling CRISPR Guide RNA design tool	Benchling	https://www.benchling.com/crispr
CHOP-CHOP	(94)	https://chopchop.cbu.uib.no/
FlowJo	BD (Becton, Dickinson & Co.)	http://www.flowjo.com
ImageJ	(95)	https://imagej.nih.gov/ij/
Other		
Eclipse Ti epifluorescence microscope	Nikon Inc.	N/A
S1000 Flow Cytometer	Stratedigm Inc.	NA

957
958

959 **Table S1. Guide RNA sequence targeted for CRISPR/Cas9 editing**

Cell line	Gene – Exon	Target Sequence
CHO-K1	SOAT1 – Exon 2	5’ AGGAACCGGCTGTCAAAATC
CHO-K1	SOAT1 – Exon 14	5’ ATAGCTCAAGCAGACAGCGA
Huh7.5	SOAT1 – Exon 6	5’ CACCAGGTCCAAACAACGGT
Huh7.5	SOAT2 – Exon 2	5’ GGTCCATTGTACCAAGTCCG

960

961 **Table S2. Primers for confirmation of CRISPR/Cas9 editing**

Cell line	Gene – Exon	Primer Sequence
CHO-K1	SOAT1 – Exon 2	Forward: 5’ CTACAAGAGCTAGTTTCAGG Reverse: 5’ CCCTGTGTGTACAGTGCCTT
CHO-K1	SOAT1 – Exon 14	Forward: 5’ TCACTCACCTTGAAGACCCA Reverse: 5’ GGGTTCCTCTCTACACACTCA
Huh7.5	SOAT1 – Exon 6	Forward: 5’ CAGCGTATTAACGTTGTGGTGT Reverse: 5’ GCCCAATGTTGAAACAGAAAAT
Huh7.5	SOAT2 – Exon 2	Forward: 5’ CAACTTCCCCTTCTAGTAGCCC Reverse: 5’ CTTTATCACCAAGCCTCACTCC

962

References

1. Brown MS, Radhakrishnan A, Goldstein JL. Retrospective on Cholesterol Homeostasis: The Central Role of Scap. Annual review of biochemistry. 2018;87:783-807.
2. Luo J, Yang H, Song BL. Mechanisms and regulation of cholesterol homeostasis. Nature reviews Molecular cell biology. 2020;21(4):225-45.
3. Goldstein JL, Brown MS. A century of cholesterol and coronaries: from plaques to genes to statins. Cell. 2015;161(1):161-72.
4. Shimano H, Sato R. SREBP-regulated lipid metabolism: convergent physiology - divergent pathophysiology. Nat Rev Endocrinol. 2017;13(12):710-30.
5. Cyster JG, Dang EV, Reboldi A, Yi T. 25-Hydroxycholesterols in innate and adaptive immunity. Nature reviews Immunology. 2014;14(11):731-43.
6. Abrams ME, Johnson KA, Perelman SS, Zhang LS, Endapally S, Mar KB, et al. Oxysterols provide innate immunity to bacterial infection by mobilizing cell surface accessible cholesterol. Nat Microbiol. 2020;5(7):929-42.
7. Zhou QD, Chi X, Lee MS, Hsieh WY, Mkrtchyan JJ, Feng AC, et al. Interferon-mediated reprogramming of membrane cholesterol to evade bacterial toxins. Nat Immunol. 2020;21(7):746-55.
8. Wang S, Li W, Hui H, Tiwari SK, Zhang Q, Croker BA, et al. Cholesterol 25-Hydroxylase inhibits SARS-CoV-2 and other coronaviruses by depleting membrane cholesterol. The EMBO journal. 2020;39(21):e106057.
9. van Meer G, Voelker DR, Feigenson GW. Membrane lipids: where they are and how they behave. Nat Rev Mol Cell Biol. 2008;9:112-24.
10. Brown MS, Goldstein JL. A receptor-mediated pathway for cholesterol homeostasis. Science. 1986;232(4746):34-47.
11. Simons K, Ikonen E. How cells handle cholesterol. Science. 2000;290(5497):1721-6.
12. McConnell HM, Radhakrishnan A. Condensed complexes of cholesterol and phospholipids. Biochimica et biophysica acta. 2003;1610(2):159-73.
13. Das A, Brown MS, Anderson DD, Goldstein JL, Radhakrishnan A. Three pools of plasma membrane cholesterol and their relation to cholesterol homeostasis. eLife. 2014;3:e02882.
14. Venkateswaran A, Laffite BA, Joseph SB, Mak PA, Wilpitz DC, Edwards PA, et al. Control of cellular cholesterol efflux by the nuclear oxysterol receptor LXRα. Proc Natl Acad Sci USA. 2000;97(22):12097-102.
15. Repa JJ, Mangelsdorf DJ. The role of orphan nuclear receptors in the regulation of cholesterol homeostasis. Annual review of cell and developmental biology. 2000;16:459-81.
16. Lange Y, Ye J, Steck TL. How cholesterol homeostasis is regulated by plasma membrane cholesterol in excess of phospholipids. Proceedings of the National Academy of Sciences of the United States of America. 2004;101(32):11664-7.
17. Infante RE, Radhakrishnan A. Continuous transport of a small fraction of plasma membrane cholesterol to endoplasmic reticulum regulates total cellular cholesterol. eLife. 2017;6:e25466.
18. Radhakrishnan A, Sun LP, Kwon HJ, Brown MS, Goldstein JL. Direct binding of cholesterol to the purified membrane region of SCAP: mechanism for a sterol-sensing domain. Molecular cell. 2004;15(2):259-68.
19. Sokolov A, Radhakrishnan A. Accessibility of cholesterol in endoplasmic reticulum membranes and activation of SREBP-2 switch abruptly at a common cholesterol threshold. J Biol Chem. 2010;285(38):29480-90.
20. Chang T-Y, Chang CY, Ohgami N, Yamauchi Y. Cholesterol sensing, trafficking, and esterification. Annu Rev Cell Dev Biol. 2006;22:129-57.

21. Xu X, Tabas I. Lipoproteins activate acyl-coenzyme A:cholesterol acyltransferase in macrophages only after cellular cholesterol pools are expanded to a critical threshold level. J Biol Chem. 1991;266(26):17040-8.
22. Chang TY, Chang CC, Cheng D. Acyl-coenzyme A:cholesterol acyltransferase. Annual review of biochemistry. 1997;66:613-38.
23. Lund EG, Kerr TA, Sakai J, Li WP, Russell DW. cDNA cloning of mouse and human cholesterol 25-hydroxylases, polytopic membrane proteins that synthesize a potent oxysterol regulator of lipid metabolism. J Biol Chem. 1998;273(51):34316-27.
24. Radhakrishnan A, Ikeda Y, Kwon HJ, Brown MS, Goldstein JL. Sterol-regulated transport of SREBPs from endoplasmic reticulum to Golgi: oxysterols block transport by binding to Insig. Proceedings of the National Academy of Sciences of the United States of America. 2007;104(16):6511-8.
25. Janowski BA, Willy PJ, Devi TR, Falck JR, Mangelsdorf DJ. An oxysterol signalling pathway mediated by the nuclear receptor LXR alpha. Nature. 1996;383(6602):728-31.
26. Brown MS, Dana SE, Goldstein JL. Cholesterol ester formation in cultured human fibroblasts. Stimulation by oxygenated sterols. J Biol Chem. 1975;250(10):4025-7.
27. Goldstein JL, Rawson RB, Brown MS. Mutant mammalian cells as tools to delineate the sterol regulatory element-binding protein pathway for feedback regulation of lipid synthesis. Arch Biochem Biophys. 2002;397(2):139-48.
28. Gay A, Rye D, Radhakrishnan A. Switch-like responses of two cholesterol sensors do not require protein oligomerization in membranes. Biophys J. 2015;108(6):1459-69.
29. Endapally S, Frias D, Grzemska M, Gay A, Tomchick DR, Radhakrishnan A. Molecular discrimination between two conformations of sphingomyelin in plasma membranes. Cell. 2019;176(5):1040-53.e17.
30. Johnson KA, Endapally S, Vazquez DC, Infante RE, Radhakrishnan A. Ostreolysin A and anthrolysin O use different mechanisms to control movement of cholesterol from the plasma membrane to the endoplasmic reticulum. J Biol Chem. 2019;294(46):17289-300.
31. Chakrabarti RS, Ingham SA, Kozlitina J, Gay A, Cohen JC, Radhakrishnan A, et al. Variability of cholesterol accessibility in human red blood cells measured using a bacterial cholesterol-binding toxin. eLife. 2017;6:e23355.
32. Ohtani Y, Irie T, Uekama K, Fukunaga N, Pitha J. Differential effects of a-, b- and g-cyclodextrins on human erythrocytes. Eur J Biochem. 1989;186:17-22.
33. Goldstein JL, Basu SK, Brown MS. Receptor-mediated endocytosis of low-density lipoprotein in cultured cells. Methods in enzymology. 1983;98:241-60.
34. Horton JD, Goldstein JL, Brown MS. SREBPs: activators of the complete program of cholesterol and fatty acid synthesis in the liver. The Journal of clinical investigation. 2002;109(9):1125-31.
35. Lehmann JM, Kliewer SA, Moore LB, Smith-Oliver TA, Oliver BB, Su JL, et al. Activation of the nuclear receptor LXR by oxysterols defines a new hormone response pathway. J Biol Chem. 1997;272(6):3137-40.
36. Janowski BA, Grogan MJ, Jones SA, Wisely GB, Kliewer SA, Corey EJ, et al. Structural requirements of ligands for the oxysterol liver X receptors LXRalpha and LXRbeta. Proceedings of the National Academy of Sciences of the United States of America. 1999;96(1):266-71.
37. Ma Y, Xu L, Rodriguez-Agudo D, Li X, Heuman DM, Hylemon PB, et al. 25-Hydroxycholesterol-3-sulfate regulates macrophage lipid metabolism via the LXR/SREBP-1 signaling pathway. Am J Physiol Endocrinol Metab. 2008;295(6):E1369-79.
38. Berrodin TJ, Shen Q, Quinet EM, Yudt MR, Freedman LP, Nagpal S. Identification of 5α, 6α-epoxycholesterol as a novel modulator of liver X receptor activity. Mol Pharmacol. 2010;78(6):1046-58.
39. Nury T, Samadi M, Varin A, Lopez T, Zarrouk A, Boumhras M, et al. Biological activities of the LXRα and β agonist, 4β-hydroxycholesterol, and of its isomer, 4α-hydroxycholesterol, on

oligodendrocytes: effects on cell growth and viability, oxidative and inflammatory status. Biochimie. 2013;95(3):518-30.
40. Cadigan KM, Heider JG, Chang TY. Isolation and characterization of Chinese hamster ovary cell mutants deficient in acyl-coenzyme A:cholesterol acyltransferase activity. J Biol Chem. 1988;263(1):274-82.
41. Chang CC, Chen J, Thomas MA, Cheng D, Del Priore VA, Newton RS, et al. Regulation and immunolocalization of acyl-coenzyme A: cholesterol acyltransferase in mammalian cells as studied with specific antibodies. J Biol Chem. 1995;270(49):29532-40.
42. Sakai J, Duncan EA, Rawson RB, Hua X, Brown MS, Goldstein JL. Sterol-regulated release of SREBP-2 from cell membranes requires two sequential cleavages, one within a transmembrane segment. Cell. 1996;85(7):1037-46.
43. Rawson RB, DeBose-Boyd R, Goldstein JL, Brown MS. Failure to cleave sterol regulatory element-binding proteins (SREBPs) causes cholesterol auxotrophy in Chinese hamster ovary cells with genetic absence of SREBP cleavage-activating protein. J Biol Chem. 1999;274(40):28549-56.
44. Lange Y, Swaisgood MH, Ramos BV, Steck TL. Plasma membranes contain half the phospholipid and 90% of the cholesterol and sphingomyelin in cultured human fibroblasts. J Biol Chem. 1989;264(7):3786-93.
45. Das A, Goldstein JL, Anderson DD, Brown MS, Radhakrishnan A. Use of mutant 125I-perfringolysin O to probe transport and organization of cholesterol in membranes of animal cells. Proceedings of the National Academy of Sciences of the United States of America. 2013;110(26):10580-5.
46. Radhakrishnan A, Goldstein JL, McDonald JG, Brown MS. Switch-like control of SREBP-2 transport triggered by small changes in ER cholesterol: a delicate balance. Cell Metab. 2008;8(6):512-21.
47. Wattenberg BW, Silbert DF. Sterol partitioning among intracellular membranes. J Biol Chem. 1983;258(4):2284-9.
48. Radhakrishnan A, McConnell HM. Chemical activity of cholesterol in membranes. Biochemistry. 2000;39(28):8119-24.
49. Lange Y, Strebel F, Steck TL. Role of the plasma membrane in cholesterol esterification in rat hepatoma cells. J Biol Chem. 1993;268(19):13838-43.
50. Brown MS, Faust JR, Goldstein JL, Kaneko I, Endo A. Induction of 3-hydroxy-3-methylglutaryl coenzyme A reductase activity in human fibroblasts incubated with compactin (ML-236B), a competitive inhibitor of the reductase. J Biol Chem. 1978;253(4):1121-8.
51. Pai JT, Guryev O, Brown MS, Goldstein JL. Differential stimulation of cholesterol and unsaturated fatty acid biosynthesis in cells expressing individual nuclear sterol regulatory element-binding proteins. J Biol Chem. 1998;273(40):26138-48.
52. Ormsby TJR, Owens SE, Clement L, Mills TJ, Cronin JG, Bromfield JJ, et al. Oxysterols Protect Epithelial Cells Against Pore-Forming Toxins. Front Immunol. 2022;13:815775.
53. Ormsby TJR, Owens SE, Horlock AD, Davies D, Griffiths WJ, Wang Y, et al. Oxysterols protect bovine endometrial cells against pore-forming toxins from pathogenic bacteria. FASEB journal : official publication of the Federation of American Societies for Experimental Biology. 2021;35(10):e21889.
54. Mosser EM, Rest RF. The Bacillus anthracis cholesterol-dependent cytolysin, Anthrolysin O, kills human neutrophils, monocytes and macrophages. BMC Microbiol. 2006;6:56.
55. Shannon JG, Ross CL, Koehler TM, Rest RF. Characterization of anthrolysin O, the Bacillus anthracis cholesterol-dependent cytolysin. Infection and immunity. 2003;71(6):3183-9.
56. Shimada Y, Maruya M, Iwashita S, Ohno-Iwashita Y. The C-terminal domain of perfringolysin O is an essential cholesterol-binding unit targeting to cholesterol-rich microdomains. European journal of biochemistry / FEBS. 2002;269(24):6195-203.

57. Tweten RK, Hotze EM, Wade KR. The Unique Molecular Choreography of Giant Pore Formation by the Cholesterol-Dependent Cytolysins of Gram-Positive Bacteria. Annu Rev Microbiol. 2015;69:323-40.
58. Portnoy DA, Auerbuch V, Glomski IJ. The cell biology of Listeria monocytogenes infection: the intersection of bacterial pathogenesis and cell-mediated immunity. J Cell Biol. 2002;158(3):409-14.
59. Radoshevich L, Cossart P. Listeria monocytogenes: towards a complete picture of its physiology and pathogenesis. Nat Rev Microbiol. 2018;16(1):32-46.
60. Abrams ME, Johnson KA, Radhakrishnan A, Alto NM. Accessible cholesterol is localized in bacterial plasma membrane protrusions. Journal of lipid research. 2020;61(12):1538.
61. Bauman DR, Bitmansour AD, McDonald JG, Thompson BM, Liang G, Russell DW. 25-Hydroxycholesterol secreted by macrophages in response to Toll-like receptor activation suppresses immunoglobulin A production. Proceedings of the National Academy of Sciences of the United States of America. 2009;106(39):16764-9.
62. Dennis EA, Deems RA, Harkewicz R, Quehenberger O, Brown HA, Milne SB, et al. A mouse macrophage lipidome. J Biol Chem. 2010;285(51):39976-85.
63. Meiner VL, Cases S, Myers HM, Sande ER, Bellosta S, Schambelan M, et al. Disruption of the acyl-CoA:cholesterol acyltransferase gene in mice: evidence suggesting multiple cholesterol esterification enzymes in mammals. Proceedings of the National Academy of Sciences of the United States of America. 1996;93(24):14041-6.
64. Wollert T, Pasche B, Rochon M, Deppenmeier S, van den Heuvel J, Gruber AD, et al. Extending the host range of Listeria monocytogenes by rational protein design. Cell. 2007;129(5):891-902.
65. Liu SY, Aliyari R, Chikere K, Li G, Marsden MD, Smith JK, et al. Interferon-inducible cholesterol-25-hydroxylase broadly inhibits viral entry by production of 25-hydroxycholesterol. Immunity. 2013;38(1):92-105.
66. Li C, Deng YQ, Wang S, Ma F, Aliyari R, Huang XY, et al. 25-Hydroxycholesterol Protects Host against Zika Virus Infection and Its Associated Microcephaly in a Mouse Model. Immunity. 2017;46(3):446-56.
67. Zu S, Deng YQ, Zhou C, Li J, Li L, Chen Q, et al. 25-Hydroxycholesterol is a potent SARS-CoV-2 inhibitor. Cell research. 2020;30(11):1043-5.
68. Zang R, Case JB, Yutuc E, Ma X, Shen S, Gomez Castro MF, et al. Cholesterol 25-hydroxylase suppresses SARS-CoV-2 replication by blocking membrane fusion. Proceedings of the National Academy of Sciences of the United States of America. 2020;117(50):32105-13.
69. Blight KJ, McKeating JA, Rice CM. Highly permissive cell lines for subgenomic and genomic hepatitis C virus RNA replication. J Virol. 2002;76(24):13001-14.
70. Sumpter R, Jr., Loo YM, Foy E, Li K, Yoneyama M, Fujita T, et al. Regulating intracellular antiviral defense and permissiveness to hepatitis C virus RNA replication through a cellular RNA helicase, RIG-I. J Virol. 2005;79(5):2689-99.
71. Pramfalk C, Jakobsson T, Verzijl CRC, Minniti ME, Obensa C, Ripamonti F, et al. Generation of new hepatocyte-like in vitro models better resembling human lipid metabolism. Biochim Biophys Acta Mol Cell Biol Lipids. 2020;1865(6):158659.
72. Kandutsch AA, Chen HW. Inhibition of sterol synthesis in cultured mouse cells by cholesterol derivatives oxygenated in the side chain. J Biol Chem. 1974;249(19):6057-61.
73. Brown MS, Goldstein JL. Suppression of 3-hydroxy-3-methylglutaryl coenzyme A reductase activity and inhibition of growth of human fibroblasts by 7-ketocholesterol. J Biol Chem. 1974;249(22):7306-14.
74. Brown AJ, Sharpe LJ, Rogers MJ. Oxysterols: From physiological tuners to pharmacological opportunities. Br J Pharmacol. 2020.
75. Russell DW. The enzymes, regulation, and genetics of bile acid synthesis. Annual review of biochemistry. 2003;72:137-74.

76. Spann NJ, Glass CK. Sterols and oxysterols in immune cell function. Nat Immunol. 2013;14(9):893-900.
77. Blanc M, Hsieh WY, Robertson KA, Kropp KA, Forster T, Shui G, et al. The transcription factor STAT-1 couples macrophage synthesis of 25-hydroxycholesterol to the interferon antiviral response. Immunity. 2013;38(1):106-18.
78. Gold ES, Diercks AH, Podolsky I, Podyminogin RL, Askovich PS, Treuting PM, et al. 25-Hydroxycholesterol acts as an amplifier of inflammatory signaling. Proceedings of the National Academy of Sciences of the United States of America. 2014;111(29):10666-71.
79. Zhao J, Chen J, Li M, Chen M, Sun C. Multifaceted Functions of CH25H and 25HC to Modulate the Lipid Metabolism, Immune Responses, and Broadly Antiviral Activities. Viruses. 2020;12(7).
80. Griffiths WJ, Wang Y. Sterols, Oxysterols, and Accessible Cholesterol: Signalling for Homeostasis, in Immunity and During Development. Front Physiol. 2021;12:723224.
81. Tabas I, Rosoff WJ, Boykow GC. Acyl coenzyme A:cholesterol acyl transferase in macrophages utilizes a cellular pool of cholesterol oxidase-accessible cholesterol as substrate. J Biol Chem. 1988;263(3):1266-72.
82. Radhakrishnan A, Rohatgi R, Siebold C. Cholesterol access in cellular membranes controls Hedgehog signaling. Nature chemical biology. 2020;16(12):1303-13.
83. Zimmerman B, Kelly B, McMillan BJ, Seegar TCM, Dror RO, Kruse AC, et al. Crystal Structure of a Full-Length Human Tetraspanin Reveals a Cholesterol-Binding Pocket. Cell. 2016;167(4):1041-51.e11.
84. Chen Y, Zhu Y, Li X, Gao W, Zhen Z, Dong D, et al. Cholesterol inhibits TCR signaling by directly restricting TCR-CD3 core tunnel motility. Molecular cell. 2022;82(7):1278-87.e5.
85. Schwarz MC, Sourisseau M, Espino MM, Gray ES, Chambers MT, Tortorella D, et al. Rescue of the 1947 Zika Virus Prototype Strain with a Cytomegalovirus Promoter-Driven cDNA Clone. mSphere. 2016;1(5).
86. Ran FA, Hsu PD, Wright J, Agarwala V, Scott DA, Zhang F. Genome engineering using the CRISPR-Cas9 system. Nat Protoc. 2013;8(11):2281-308.
87. Sanjana NE, Shalem O, Zhang F. Improved vectors and genome-wide libraries for CRISPR screening. Nature methods. 2014;11(8):783-4.
88. Schoggins JW, Wilson SJ, Panis M, Murphy MY, Jones CT, Bieniasz P, et al. A diverse range of gene products are effectors of the type I interferon antiviral response. Nature. 2011;472(7344):481-5.
89. Johnson KA, Radhakrishnan A. The use of anthrolysin O and ostreolysin A to study cholesterol in cell membranes. Methods in enzymology. 2021;649:543-66.
90. Endapally S, Infante RE, Radhakrishnan A. Monitoring and modulating intracellular cholesterol trafficking using ALOD4, a cholesterol-binding protein. Methods in molecular biology (Clifton, NJ). 2019;1949:153-63.
91. McDonald JG, Smith DD, Stiles AR, Russell DW. A comprehensive method for extraction and quantitative analysis of sterols and secosteroids from human plasma. Journal of lipid research. 2012;53(7):1399-409.
92. Yang J, Brown MS, Ho YK, Goldstein JL. Three different rearrangements in a single intron truncate sterol regulatory element binding protein-2 and produce sterol-resistant phenotype in three cell lines. Role of introns in protein evolution. J Biol Chem. 1995;270(20):12152-61.
93. Bishop DK, Hinrichs DJ. Adoptive transfer of immunity to Listeria monocytogenes. The influence of in vitro stimulation on lymphocyte subset requirements. J Immunol. 1987;139(6):2005-9.
94. Labun K, Montague TG, Krause M, Torres Cleuren YN, Tjeldnes H, Valen E. CHOPCHOP v3: expanding the CRISPR web toolbox beyond genome editing. Nucleic Acids Res. 2019;47(W1):W171-w4.

95. Schneider CA, Rasband WS, Eliceiri KW. NIH Image to ImageJ: 25 years of image analysis. Nature methods. 2012;9(7):671-5.

Figure 1

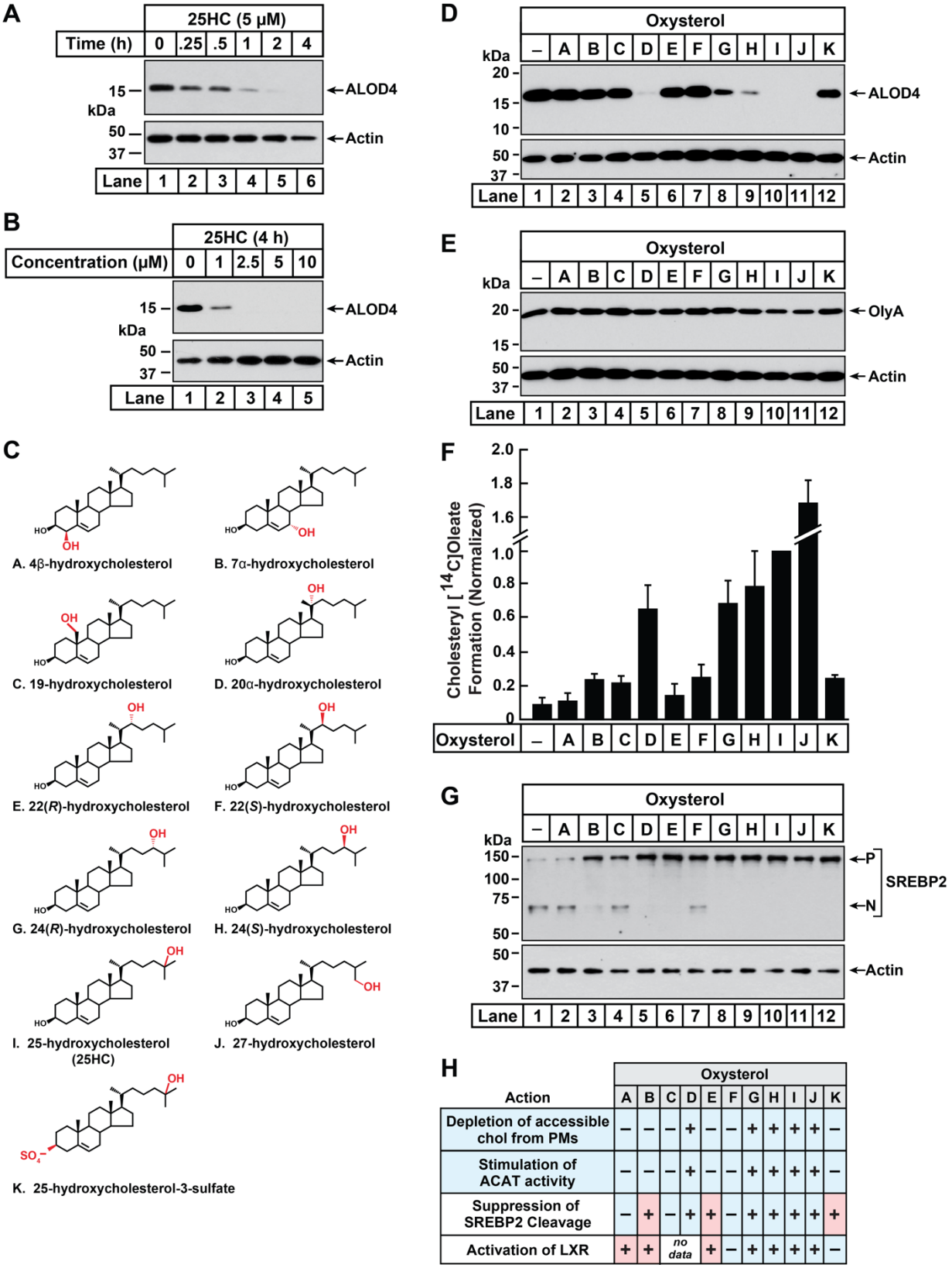

H

Action	Oxysterol										
	A	B	C	D	E	F	G	H	I	J	K
Depletion of accessible chol from PMs	–	–	–	+	–	–	+	+	+	+	–
Stimulation of ACAT activity	–	–	–	+	–	–	+	+	+	+	–
Suppression of SREBP2 Cleavage	–	+	–	+	+	–	+	+	+	+	+
Activation of LXR	+	+	*no data*	+	–	+	+	+	+	+	–

Figure 1. Comparison of oxysterol specificities for effects on PM cholesterol pools, stimulation of ACAT activity, and suppression of SREBP-2 cleavage.

(A, B) Time course and dose curve analysis of 25HC treatment. On day 0, CHO-K1 cells were set up in medium B at a density of 6 x 10^4 cells per well of a 48-well plate. On day 1, media was removed, cells were washed twice with 500 µl of PBS followed by addition of 200 µl of medium B supplemented with either 5 µM of 25HC (A) or the indicated concentrations of 25HC (B). After incubation at 37°C for either the indicated times (A) or 4 h (B), media was removed and replaced with 200 µl of medium B supplemented with 3 µM His_6-Flag-ALOD4. After incubation at 37°C for 30 min, cells were washed twice with 500 µl of PBS, harvested, and equal aliquots of cell lysates were subjected to immunoblot analysis as described in *Methods*.

(C) Chemical structures of oxysterols tested in this study. Differences from cholesterol are highlighted in *red*.

(D, E) Effects on PM cholesterol pools. On day 0, CHO-K1 cells were set up in medium B at a density of 6 x 10^4 cells per well of a 48-well plate. On day 1, media was removed, cells were washed twice with 500 µl of PBS followed by addition of 200 µl of medium B supplemented with 5 µM of the indicated oxysterol. After incubation at 37°C for 4 h, media was removed and replaced with 200 µl of medium B supplemented with 3 µM of either His_6-Flag-ALOD4 (D*, top panel*) or OlyA-His_6 (E*, top panel*). After incubation at 37°C for 30 min, cells were washed twice with 500 µl of PBS, harvested, and equal aliquots of cell lysates were subjected to immunoblot analysis as described in *Methods*.

(F) ACAT activity. On day 0, CHO-K1 cells were set up in medium B at a density of 2.5 x 10^5 cells per 60-mm dish. On day 2, media was removed, cells were washed twice with 1 ml of PBS followed by addition of 2 ml of cholesterol-depleting medium C. On day 3, media was removed, cells were washed with 1 ml of PBS followed by addition of 1 ml of medium C supplemented with 5 µM of the indicated oxysterol. After incubation at 37°C for 1 h, each dish was supplemented with 0.2 mM sodium [^{14}C]oleate (6500 dpm/nmol) and incubated at 37°C for an additional 2 h, after which cells were harvested, and levels of cholesteryl [^{14}C]oleate were measured as described in *Methods*. Each column represents the mean of cholesterol esterification measurements from three or more independent experiments, and error bars show the standard error. The mean value for cholesterol esterification obtained after 25HC treatment (3.18 nmol/mg/h; n = 6; standard error = ± 0.49 nmol/mg/h) was set to 1 and all other values were normalized relative to this set-point.

(G) SREBP-2 cleavage. On day 0, CHO-K1 cells were set up in medium B at a density of 6 x 10^4 cells per well of a 48-well plate. On day 1, media was removed, cells were washed twice with

500 µl of PBS followed by addition of 200 µl of cholesterol-depleting medium C supplemented with 1% (w/v) HPCD. After incubation at 37°C for 1 h, media was removed, cells were washed twice with 500 µl of PBS and then treated with 200 µl of medium C supplemented with 5 µM of the indicated oxysterol. After incubation at 37°C for 4 h, cells were washed twice with 500 µl of PBS, harvested, and equal aliquots of cell lysates were subjected to immunoblot analysis as described in *Methods*. *P*, precursor form of SREBP2; *N*, cleaved nuclear form of SREBP2.

(H) Summary of oxysterol specificities for depletion of accessible cholesterol from PMs, suppression of SREBP2 cleavage, activation of LXR transcription factors, and stimulation of ACAT activity. The degree of effect (maximal or minimal) is denoted by + and –, respectively. Specificities that are different from that for depletion of accessible cholesterol from PMs (first row) are shaded *red*.

Figure 2

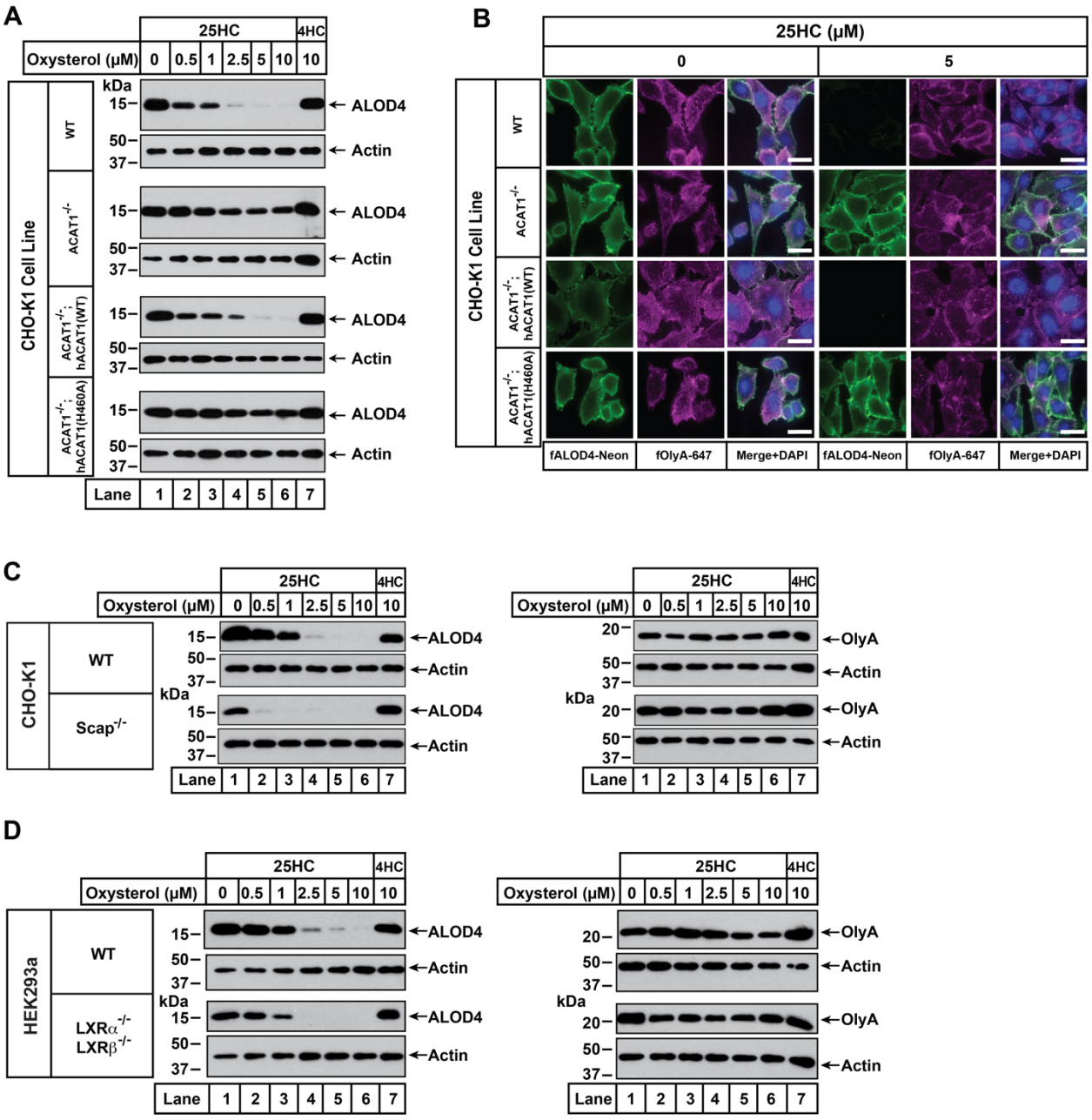

Figure 2. 25HC fails to trigger rapid depletion of accessible cholesterol from PMs of ACAT-deficient cells.

(A) Immunoblot analysis of ALOD4 binding. On day 0, the indicated versions of CHO-K1 cells were set up in medium B at a density of 6 x 10^4 cells per well of a 48-well plate. On day 1, media was removed, cells were washed twice with 500 μl of PBS followed by addition of 200 μl of

medium B supplemented with the indicated concentrations of either 25HC or 4HC. After incubation at 37°C for 4 h, media was removed and replaced with 200 µl of medium B supplemented with 3 µM His_6-Flag-ALOD4. After incubation at 37°C for 30 min, cells were washed twice with 500 µl of PBS, harvested, and equal aliquots of cell lysates were subjected to immunoblot analysis as described in *Methods*.

(B) Fluorescence microscopy analysis of ALOD4 and OlyA binding. On day 0, the indicated versions of CHO-K1 cells were set up in medium B at a density of 3 x 10^4 cells per well of an 8-well Lab-Tek II chambered #1.5 coverglass dish. On day 1, media was removed, cells were washed twice with 500 µl of PBS followed by addition of 200 µl of medium B supplemented with the indicated concentration of 25HC. After incubation at 37°C for 4 h, media was removed and replaced with 200 µl of medium B supplemented with 3 µM of either fALOD4-Neon or fOlyA-647. After incubation at 37°C for 30 min, media was removed, cells were washed twice with 500 µl of PBS, fixed, stained with DAPI, and imaged as described in *Methods*. *Scale bar*, 25 µm.

(C, D) Effects of 25HC on PM cholesterol pools in cells lacking Scap or LXR transcription factors. On day 0, the indicated cell lines were set up in either medium B (C) or medium D (D) at a density of 6 x 10^4 cells per well of a 48-well plate. On day 1, media was removed, cells were washed twice with 500 µl of PBS followed by addition of 200 µl of media supplemented with the indicated concentrations of either 25HC (*lanes 1-6*) or 4HC (*lane 7*). After incubation at 37°C for 4 h, media was removed and replaced with 200 µl of media supplemented with 3 µM of either His_6-Flag-ALOD4 (*left panels*) or OlyA-His_6 (*right panels*). After incubation at 37°C for 30 min, cells were washed twice with 500 µl of PBS, harvested, and equal aliquots of cell lysates were subjected to immunoblot analysis as described in *Methods*.

Figure 3

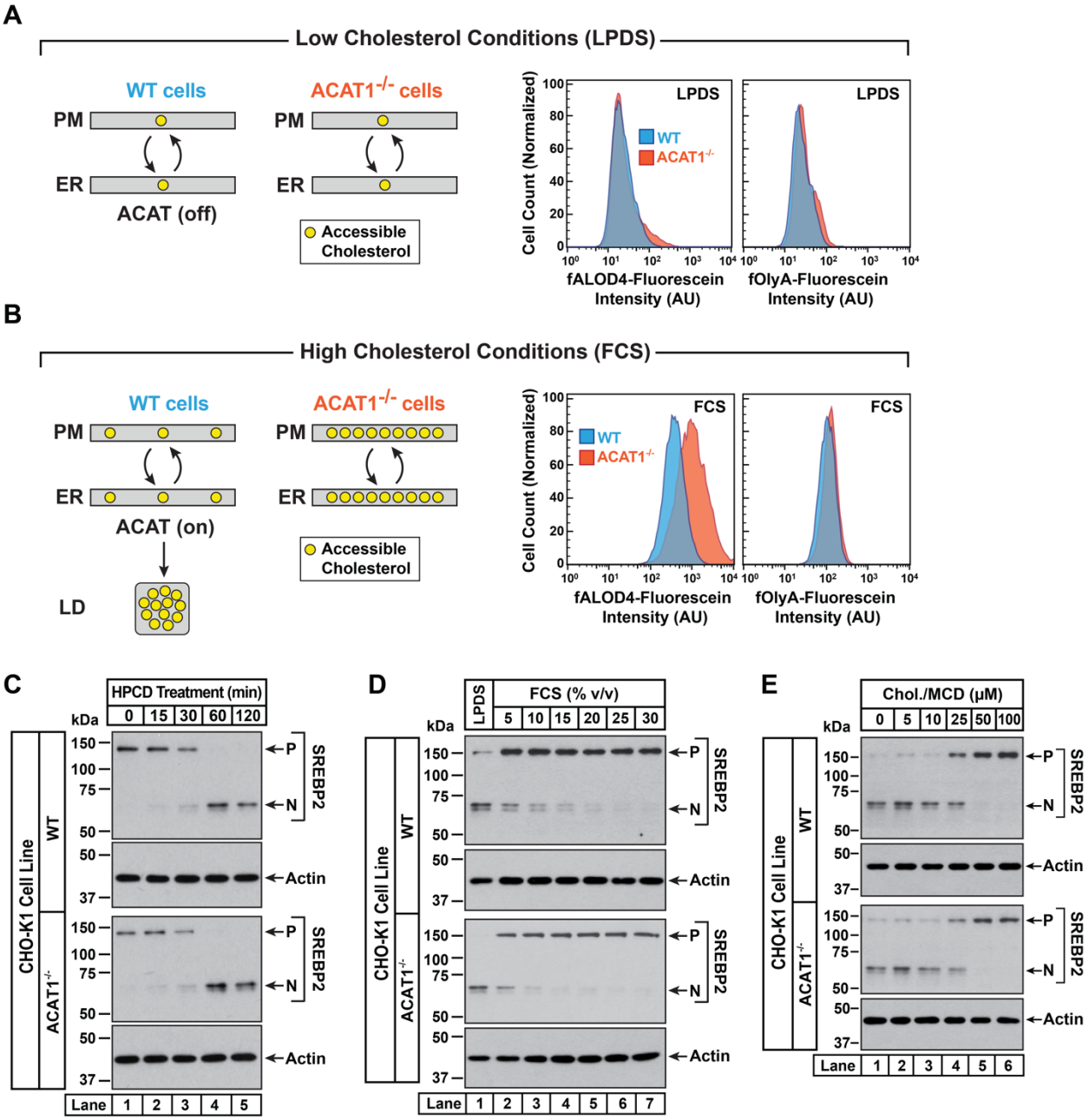

Figure 3. Intracellular cholesterol trafficking and steady state levels of PM accessible cholesterol in ACAT-deficient cells.

On day 0, wild-type and ACAT1-deficient CHO-K1 cells were set up in medium B at a density of 5 x 10^4 cells per well of a 24-well plate (A – C) or 6 x 10^4 cells per well of a 48-well plate (D, E).

(A, B) Steady state levels of accessible cholesterol in PMs. On day 1, media was removed, cells were washed twice with 500 µl of PBS followed by addition of 500 µl of medium A supplemented with 5% (v/v) of either LPDS (A) or FCS (B). On day 2, media was removed, cells were washed twice with 500 µl of PBS followed by addition of 200 µl of medium A containing 5% (v/v) of the indicated serum along with 0.5 µM of either fALOD4-fluorescein or fOlyA-fluorescein. After incubation at 37°C for 30 min, media was removed, cells were washed twice with 500 µl of PBS, and subjected to flow cytometry as described in *Methods*.

(C) Cholesterol depletion by HPCD. On day 1, media was removed, cells were washed twice with 500 µl of PBS followed by addition of 200 µl of medium B supplemented with 2% (w/v) HPCD.

(D) Cholesterol repletion by lipoproteins. On day 1, media was removed, cells were washed twice with 500 µl of PBS followed by addition of 500 µl of cholesterol-depleting medium C. On day 2, media was removed, cells were washed twice with 500 µl of PBS followed by addition of 200 µl of either medium A containing either 5% (v/v) lipoprotein-deficient serum (*lane 1*) or the indicated concentrations of lipoprotein-rich FCS (*lanes 2 – 7*).

(E) Cholesterol repletion by cholesterol/cyclodextrin complexes. On day 1, media was removed, cells were washed twice with 500 µl of PBS followed by addition of 200 µl of medium C supplemented with 1% (w/v) HPCD. After incubation at 37°C for 1 h, media was removed, cells were washed twice with 500 µl of PBS followed by addition of 200 µl of medium C supplemented with the indicated concentrations of cholesterol/MCD complexes.

(C – E) After incubation at 37°C for the indicated times (C), 5 h (D), or 3 h (E), media was removed, cells were washed twice with 500 µl of PBS, harvested, and equal aliquots of cell lysates were subjected to immunoblot analysis as described in *Methods*. *P*, precursor form of SREBP2; *N*, cleaved nuclear form of SREBP2.

Figure 4

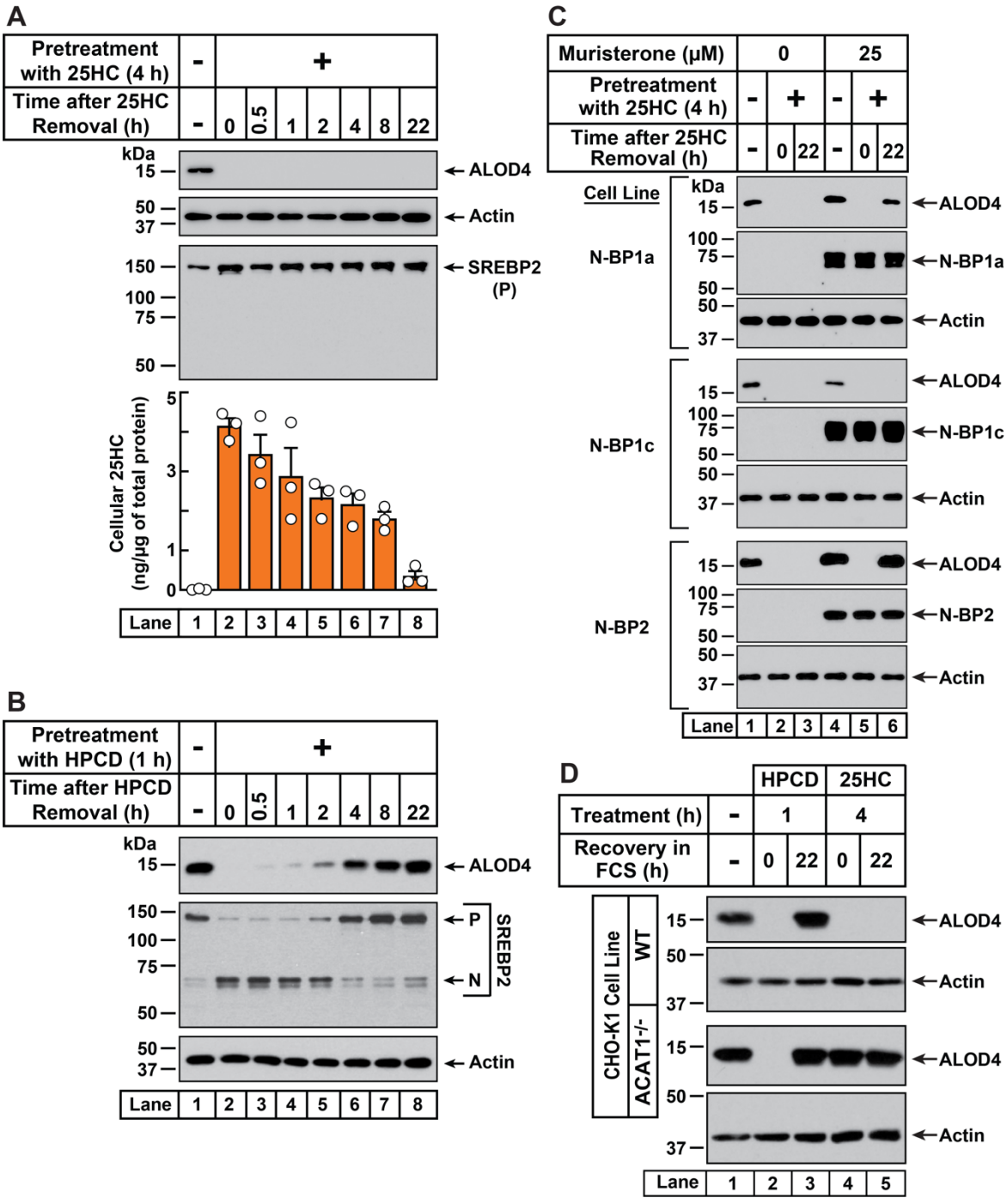

Figure 4. 25HC-triggered depletion of accessible cholesterol from PMs persists for long times through suppression of SREBP-mediated cholesterol synthesis and uptake

(A) Retention of 25HC in cells prevents replenishment of accessible cholesterol on PMs after it has been depleted by 25HC. On day 0, CHO-K1 cells were set up in medium B in eight 24-well plates at a density of 1.5 x 10^5 cells per well. On day 1, media was removed from seven of the eight plates, cells were washed twice with 1 ml of PBS followed by addition of 1 ml of medium B supplemented with 5 μM of 25HC (*lanes 2-8*). After incubation at 37°C for 4 h, media was removed, cells were washed twice with 1 ml of PBS followed by addition of 1 ml of medium B. Each of the seven plates was incubated for the indicated times, after which media was removed from 10 wells and cells were washed twice with 1 ml of PBS. Then, 100 μl of PBS was added to each well and the cells were scraped and pooled for further analysis. The eighth plate (*lane 1*) was not subjected to any treatment and was processed for analysis as above. For each plate, an aliquot of the pooled cells (20% of total) was used to determine protein concentration with a BCA protein assay kit and the remainder (80% of total) was subjected to mass spectrometry analysis as described in *Methods*. An eleventh well from each plate was subjected to immunoblot analysis of His_6-Flag-ALOD4 binding (*top panel*). These samples were also immunoblotted for SREBP2 (*third panel*). P, precursor form of SREBP2; N, cleaved nuclear form of SREBP2.

(B) Recovery of accessible cholesterol on PMs after depletion by HPCD. On day 0, CHO-K1 cells were set up in medium B at a density of 1.5 x 10^5 cells per well of a 24-well plate. On day 1, media was removed, cells were washed twice with 1 ml of PBS followed by addition of 300 μl of medium B supplemented with 1% (w/v) HPCD (*lanes 2-8*). After incubation at 37°C for 1 h, media was removed, cells were washed twice with 1 ml of PBS followed by addition of 1 ml of medium B. After incubation for the indicated times, media was removed from these treated wells as well as from a well that was not subjected to any of the above treatments (*lane 1*). The media was replaced with 200 μl of medium B supplemented with 3 μM His_6-Flag-ALOD4. After incubation at 37°C for 30 min, cells were washed twice with 1 ml of PBS, harvested, and equal aliquots of cell lysates were subjected to immunoblot analysis as described in *Methods*.

(C) Nuclear SREBPs counteract 25HC-mediated depletion of accessible cholesterol. On day 0, Site-2 protease-deficient CHO-K1 cells inducibly expressing the nuclear transcription factor domains (N-BP) of the indicated isoforms of SREBP were set up in medium B at a density of 5 x 10^4 cells per well of a 48-well plate. On day 1, media was removed, cells were washed twice with 500 μl of PBS followed by addition of 200 μl of medium B supplemented with the indicated concentrations of muristerone A. On day 2, media was removed, cells were washed twice with 500 μl of PBS followed by addition of 200 μl of medium B supplemented with the indicated

concentration of muristerone along with 5 μM 25HC (*lanes 2, 3, 5, 6*). After incubation at 37°C for 4 h, media was removed, cells were washed twice with 500 μl of PBS followed by addition of 200 μl of medium B. After incubation for the indicated times, media was removed from these 25HC-treated wells as well as from two wells that were not subjected to any of the above treatments (*lanes 1, 4*). The media was replaced with 200 μl of medium B supplemented with 3 μM His_6-Flag-ALOD4. After incubation at 37°C for 30 min, cells were washed twice with 500 μl of PBS, harvested, and equal aliquots of cell lysates were subjected to immunoblot analysis as described in *Methods*.

(D) PM accessible cholesterol in ACAT-deficient cells. On day 0, the indicated versions of CHO-K1 cells were set up in medium B at a density of 1.5 x 10^5 cells per well of a 24-well plate. On day 1, media was removed, cells were washed twice with 500 μl of PBS followed by addition of 300 μl of medium B supplemented with either 1% (w/v) HPCD (*lanes 2, 3*) or 5 μM 25HC (*lanes 4, 5*). After incubation for either 1 h (*lanes 2, 3*) or 4 h (*lanes 4, 5*), media was removed, cells were washed twice with PBS followed by addition of 1 ml of medium B. After incubation for the indicated times, media was removed from these treated wells as well as from a well that was not subjected to any of the above treatments (*lane 1*). The media was replaced with 200 μl of medium B supplemented with 3 μM His_6-Flag-ALOD4. After incubation at 37°C for 30 min, cells were washed twice with 1 ml of PBS, harvested, and equal aliquots of cell lysates were subjected to immunoblot analysis as described in *Methods*.

Figure 5

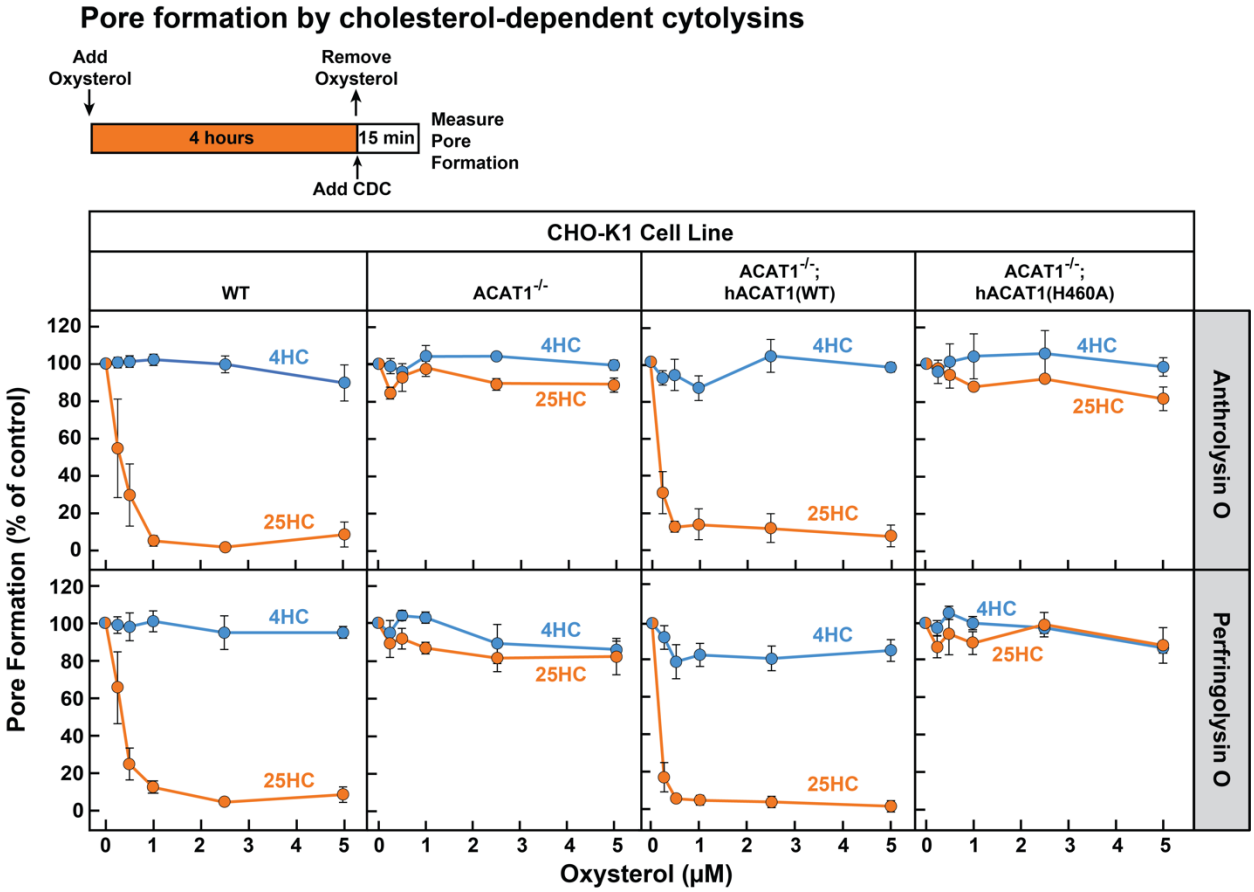

Figure 5. 25HC fails to protect ACAT-deficient cells from pore formation by bacterial cytolysins.

Pore formation by bacterial cytolysins. On day 0, the indicated versions of CHO-K1 cells were set up in medium B at a density of 7.5 x 10^4 cells per well of a 48-well plate. On day 1, media was removed and replaced with 500 µl of medium B supplemented with the indicated concentrations of either 25HC or 4HC. After incubation at 37°C for 4 h, media was removed, cells were washed twice with 500 µl of HBSS followed by addition of 500 µl of HBSS containing either 100 pM of His_6-ALO(FL) (top panel) or 500 pM of His_6-PFO(FL) (bottom panel). After incubation at 37°C for 15 min, media was removed and pore formation was assessed as described in *Methods*. For each cell line, the extent of pore formation in the absence of oxysterol treatment was set to 100%, and all other values were normalized to this set-point.

Figure 6

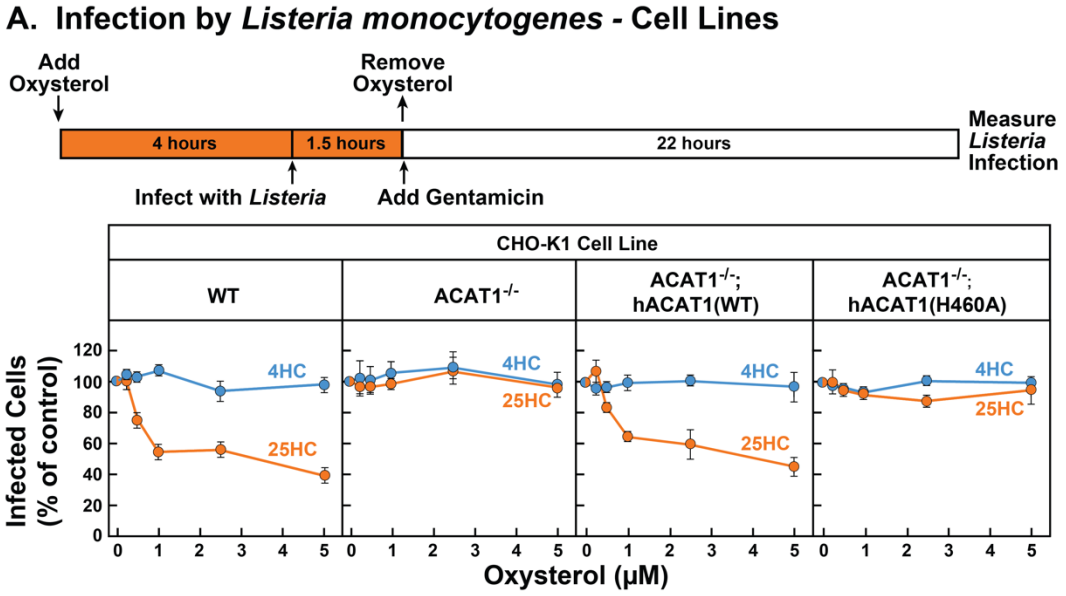

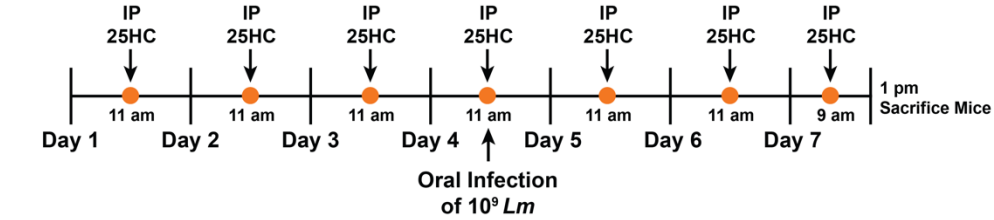

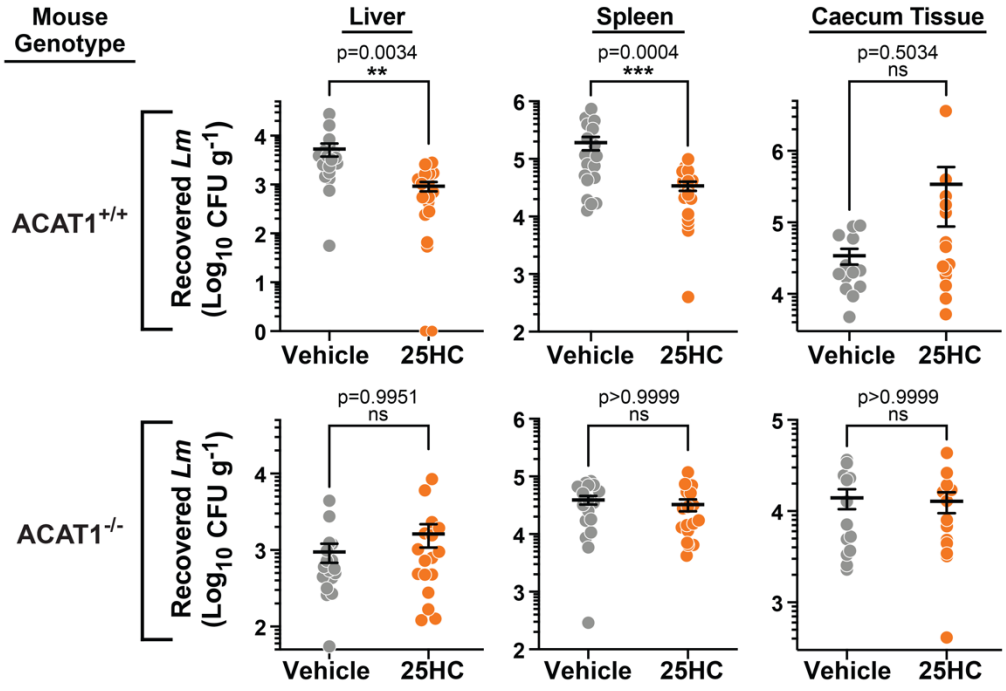

1398

Figure 6. 25HC fails to protect ACAT-deficient cell lines and mice from infection by *Listeria monocytogenes*

(A) *Listeria* infection of CHO-K1 cells. On day 0, the indicated versions of CHO-K1 cells were set up in medium I at a density of 1 x 10^5 cells per well of a 24-well plate. On day 1, media was supplemented with either 25HC or 4HC to obtain the final concentration indicated. After incubation at 37°C for 4 h, cells were infected with *Listeria monocytogenes* (MOI = 1) for 90 min. Following this step, cells were washed twice with 1 ml of PBS followed by addition of 1 ml of medium I supplemented with 50 µg/ml of gentamicin to kill extracellular bacteria. After 22 h, cells were harvested and infection levels were determined as described in *Methods*. For each cell line, the infection level measured in the absence of oxysterols was set to 100% for each replicate, and all other values were normalized to this set-point.

(B) *Listeria* infection of mice. On days 1 – 7, ACAT1$^{+/+}$ and ACAT1$^{-/-}$ mice were injected once daily intraperitoneally with either 25HC or ethanol. On day 4, the mice were orally infected with 1 x 10^9 *Listeria monocytogenes* strain EGD harboring a mutation in Internalin A (*Lm*-InlA^m) as described in the *Methods*. On day 7, 4 h after the 25HC injection, the spleen, liver, and caecum tissues of each mouse was collected and infection levels were determined as described in *Methods*. Asterisks denote levels of statistical significance (one-way analysis of variance (ANOVA) with Dunnett's correction): non-significant (ns) $p>0.05$; * $p\leq0.05$; ** $p\leq0.01$; and *** $p\leq0.001$. *IP*, intraperitoneal injection.

Figure 7

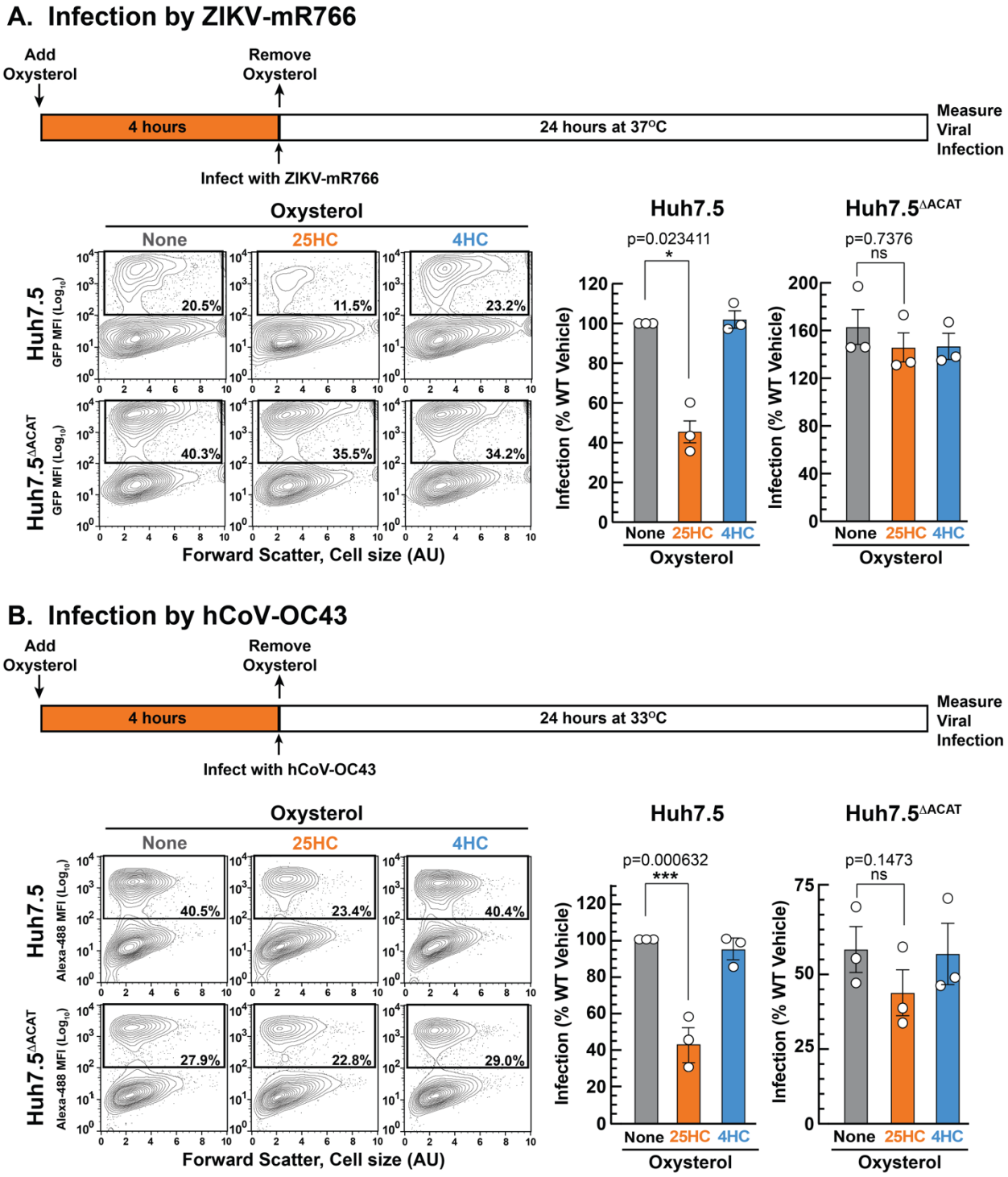

Figure 7. 25HC fails to protect ACAT-deficient cells from viral infection.

(A, B) Viral infection of Huh7.5 cells. On day 0, the indicated versions of Huh7.5 cells were set

up in medium E at a density of 7 x 10^4 cells per well of a 24-well plate. On day 1, media was removed and replaced with 1 ml of medium E supplemented with 5 μM of the indicated oxysterol. After incubation at 37°C for 4 h, media was removed, and cells were infected with either hCoV-OC43 (A) or ZIKV-mR766 (B) at the indicated temperatures as described in *Methods*. After 24 h, cells were harvested, and infection levels were determined as described *in Material and Methods*. Representative flow cytometry plots of infected cells and quantification of infection levels (*rectangular boxes*) are shown for hCoV-OC43 (A) and ZIKV-mR766 (B). The infection value obtained for Huh7.5 cells in the absence of oxysterol treatment for each experiment was set to 100% and all other values are normalized to this set-point. Asterisks denote levels of statistical significance (one-way analysis of variance (ANOVA) with Dunnett's correction) of the unnormalized data: non-significant (ns) $p>0.05$; * $p\leq0.05$; ** $p\leq0.01$; and *** $p\leq0.001$. In all panels, no significant differences ($p>0.05$) were detected in cells treated with 4HC.

Figure S1

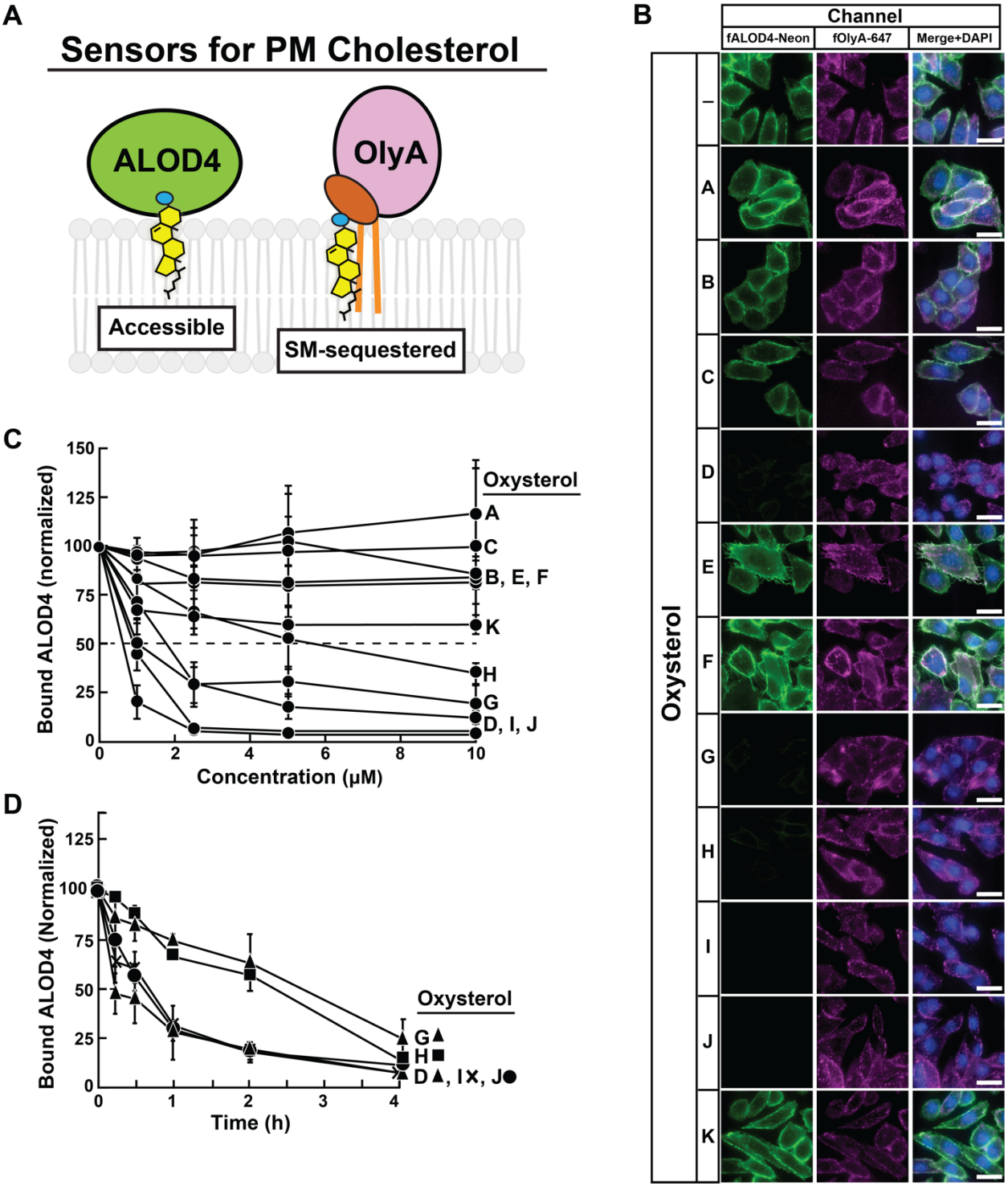

Figure S1. Comparison of effects of oxysterols on PM cholesterol pools.

(A) Schematic of protein sensors used to monitor changes in PM cholesterol pools.

(B) Fluorescence microscopy analysis of ALOD4 and OlyA binding. On day 0, CHO-K1 cells were set up in medium B at a density of 3 x 10^4 cells per well of an 8-well Lab-Tek II chambered #1.5 coverglass dish. On day 1, media was removed, cells were washed twice with 500 µl of PBS followed by addition of 200 µl of medium B supplemented with 5 µM of the indicated oxysterol. After incubation at 37°C for 4 h, media was removed and replaced with 200 µl of medium B supplemented with 3 µM fALOD4-Neon and 3 µM fOlyA-647. After incubation at 37°C for 30 min, media was removed, cells were washed twice with 500 µl of PBS, fixed, stained with DAPI, and imaged as described in *Methods*. *Scale bar*, 25 µm.

(C,D) Quantification of immunoblot analysis of ALOD4 binding. On day 0, CHO-K1 cells were set up in medium B at a density of 6 x 10^4 cells per well of a 48-well plate. On day 1, media was removed, cells were washed twice with 500 µl of PBS followed by addition of 200 µl of medium B supplemented with either varying concentrations (C) or 5 µM (D) of the indicated oxysterol. After incubation at 37°C for either 4 h (C) or for the indicated times (D), media was removed and replaced with 200 µl of medium B supplemented with 3 µM His_6-Flag-ALOD4. After incubation at 37°C for 30 min, cells were washed twice with 500 µl of PBS and harvested, after which equal aliquots of cell lysates were subjected to immunoblot analysis as described in *Methods*. The immunoblot signals for bound ALOD4 and cellular actin after treatment with various oxysterols, examples of which are shown in Figure 1A and 1B for oxysterol I, were then quantified as described in *Methods*. Data points represent the mean of 3-6 experiments and error bars show the standard error.

Figure S2

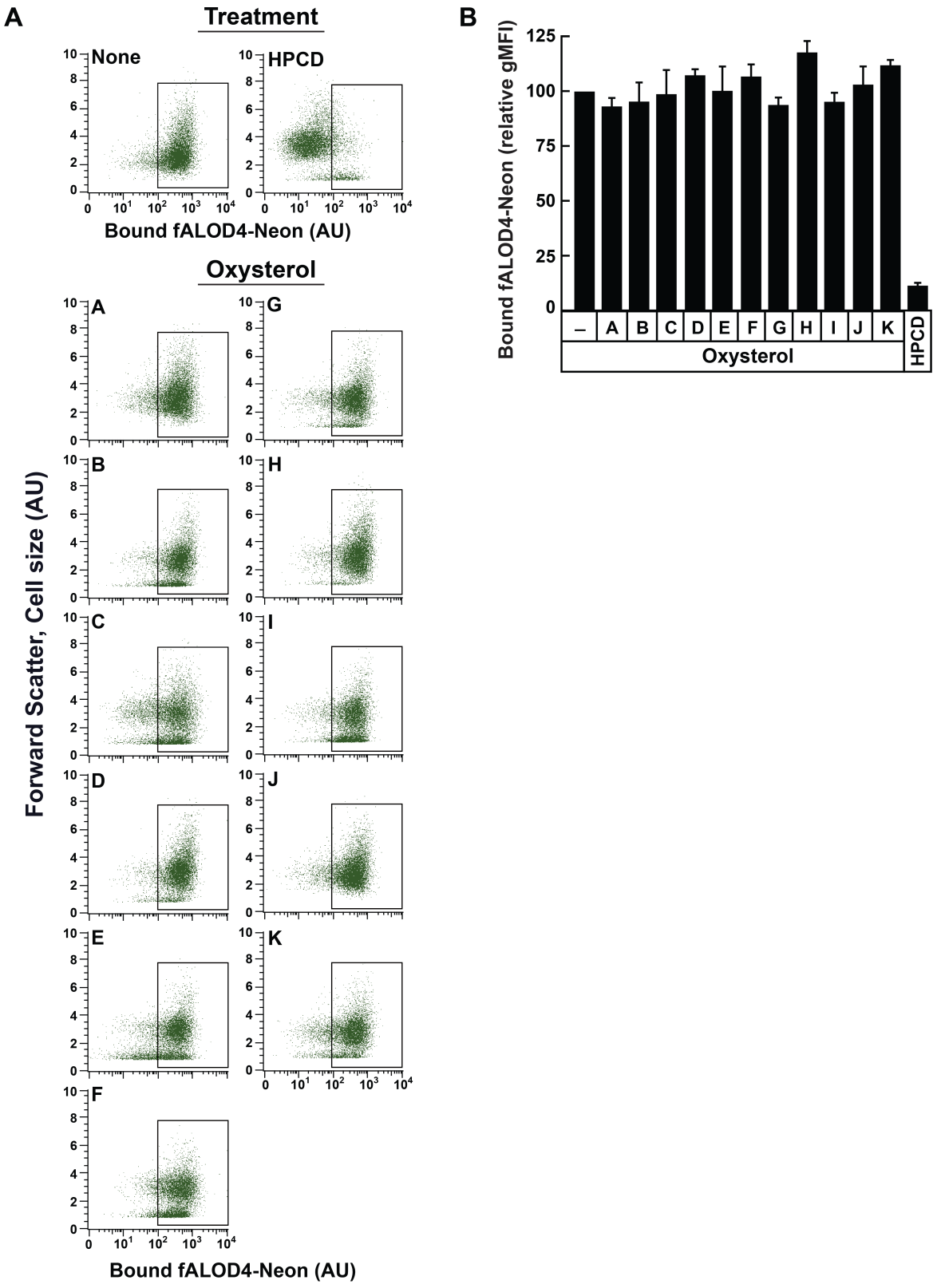

1460

Figure S2. Treatment of red blood cells with oxysterols does not affect levels of accessible cholesterol in their membranes.

(A, B) Each binding assay contained 500 µl of rabbit red blood cells (RBCs) that had been washed and diluted as described in Methods. RBCs were then subjected to one of the following treatments at room temperature (RT): i) incubation for 4 h without or with 5 µM of the indicated oxysterol solubilized either in ethanol (*A* – *J*) or DMSO (*K*); or ii) incubation for 1 h with 1% (w/v) HPCD (in buffer F). After the indicated treatments, RBCs were incubated with 1 µM of fALOD4-Neon for 30 min at RT, following which FACS analysis was carried out as described in Methods. Representative flow cytometry analysis of fALOD4-Neon binding to 10,000 RBCs are shown in (A) and the rectangular boxes represent fALOD4-Neon-bound RBCs. The geometric mean fluorescence intensity (gMFI) of Neon fluorescence from three independent experiments are shown in (B). Each column in (B) represents the mean of 3 independent experiments and error bars indicate the standard error. The mean gMFI value obtained for binding of fALOD4-Neon to RBCs in the absence of oxysterol treatment for each experiment (top left panel in A) was set to 100 and all other values were normalized to this set-point.

Figure S3

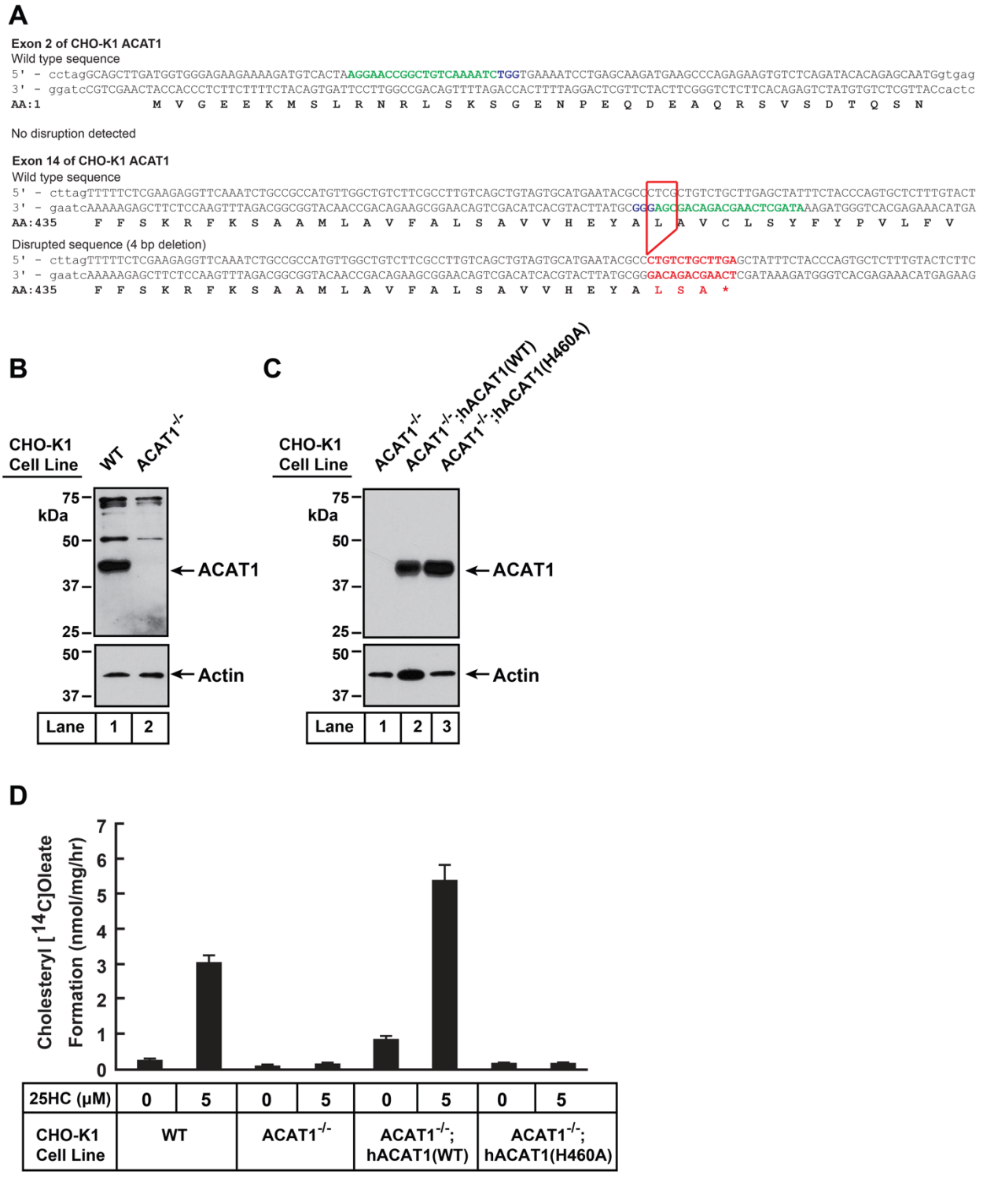

1477
1478

Figure S3. Characterization of a CHO-K1 cell line deficient in ACAT1.

(A) Strategy for generating ACAT1-deficient CHO-K1 cells using CRISPR-Cas9 technology. Two guide RNAs were designed to target and disrupt exons 2 and 14 of hamster ACAT1 (also designated as SOAT1). The 20-nucleotide target sequence is shown in green and the NGG PAM sequence is in purple. Genomic sequencing revealed no disruptions to exon 2 and a 4-bp deletion in exon 14 (*red box*) that resulted in a truncated transcript encoding amino acids 1 – 461 of ACAT1 followed by two residues (*red*) and a stop codon (*).

(B, C) Immunoblot analysis. On day 0, the indicated versions of CHO-K1 cells were set up in medium B at a density of 6 x 10^4 cells per well of a 48-well plate. On day 1, media was removed, cells were washed twice with 500 µl of PBS, harvested, and equal aliquots of cell lysates were subjected to immunoblot analysis as described in *Methods*.

(D) ACAT activity. On day 0, the indicated versions of CHO-K1 cells were set up in medium B at a density of 2.5 x 10^5 cells per 60-mm dish. On day 2, media was removed, cells were washed twice with 1 ml of PBS followed by addition of 2 ml of cholesterol-depleting medium C. On day 3, media was removed, cells were washed with 1 ml of PBS followed by addition of 1 ml of medium C supplemented with the indicated concentration of 25HC. After incubation at 37°C for 1 h, each dish was supplemented with 0.2 mM sodium [^{14}C]oleate (6500 dpm/nmol) and incubated at 37°C for an additional 2 h, after which cells were harvested, and levels of cholesteryl [^{14}C]oleate were measured as described in *Methods*. Each column represents the mean of cholesterol esterification measurements from three experiments, and error bars show the standard error.

Figure S4

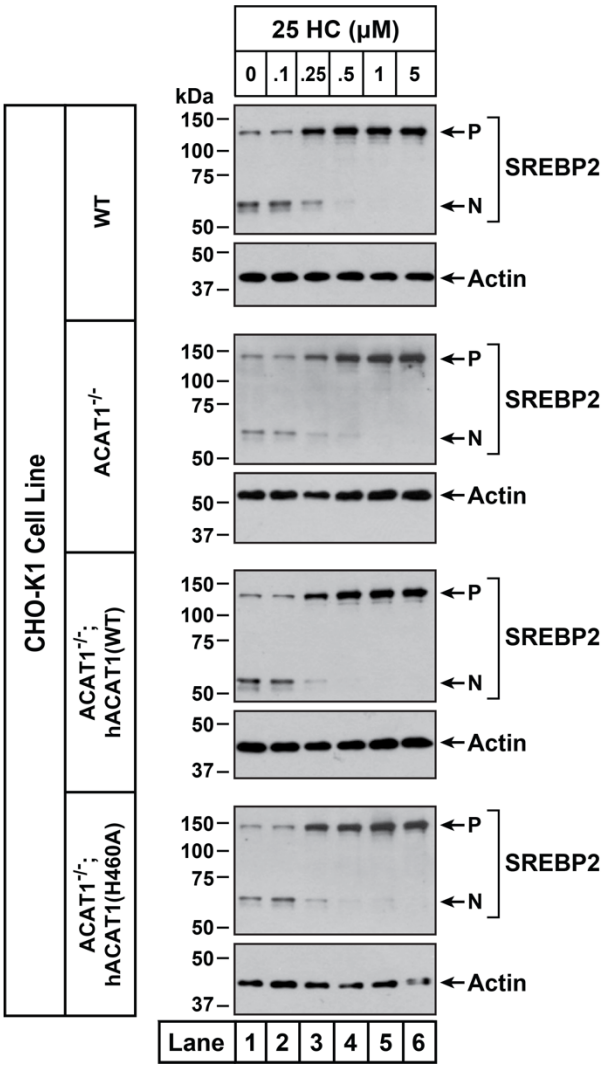

Figure S4. Effects of 25HC on SREBP2 processing in ACAT-deficient cells.

On day 0, the indicated versions of CHO-K1 cells were set up in medium B at a density of 6 x 10^4 cells per well of a 48-well plate. On day 1, media was removed, cells were washed twice with 500 μl of PBS followed by addition of 200 μl of medium C supplemented with 1% (w/v) HPCD. After incubation at 37°C for 1 h, media was removed, cells were washed twice with 500 μl of PBS followed by addition of 200 μl of medium C supplemented with the indicated concentrations of 25HC. After incubation at 37°C for 3 h, media was removed, cells were washed twice with 500 μl of PBS, harvested, and equal aliquots of cell lysates were subjected to immunoblot analysis as described in *Methods*. *P*, precursor form of SREBP2; *N*, cleaved nuclear form of SREBP2.

Figure S5

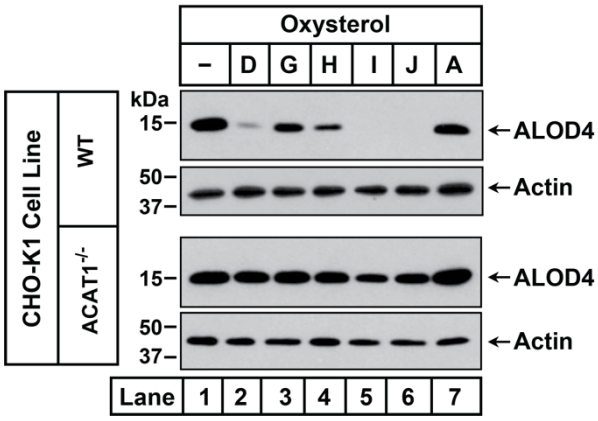

Figure S5. Oxysterols that activate ACAT fail to trigger rapid depletion of accessible cholesterol from PMs of ACAT-deficient cells.

On day 0, the indicated versions of CHO-K1 cells were set up in medium B at a density of 6 x 10^4 cells per well of a 48-well plate. On day 1, media was removed, followed by addition of 200 µl of medium B supplemented without or with 5 µM of the indicated oxysterols (see ***Figure 1C*** for oxysterol structures). After incubation at 37°C for 4 h, media was removed and replaced with 200 µl of medium B supplemented with 3 µM His_6-Flag-ALOD4. After incubation at 37°C for 30 min, cells were washed twice with 500 µl of PBS, harvested, and equal aliquots of cell lysates were subjected to immunoblot analysis as described in *Methods*.

Figure S6

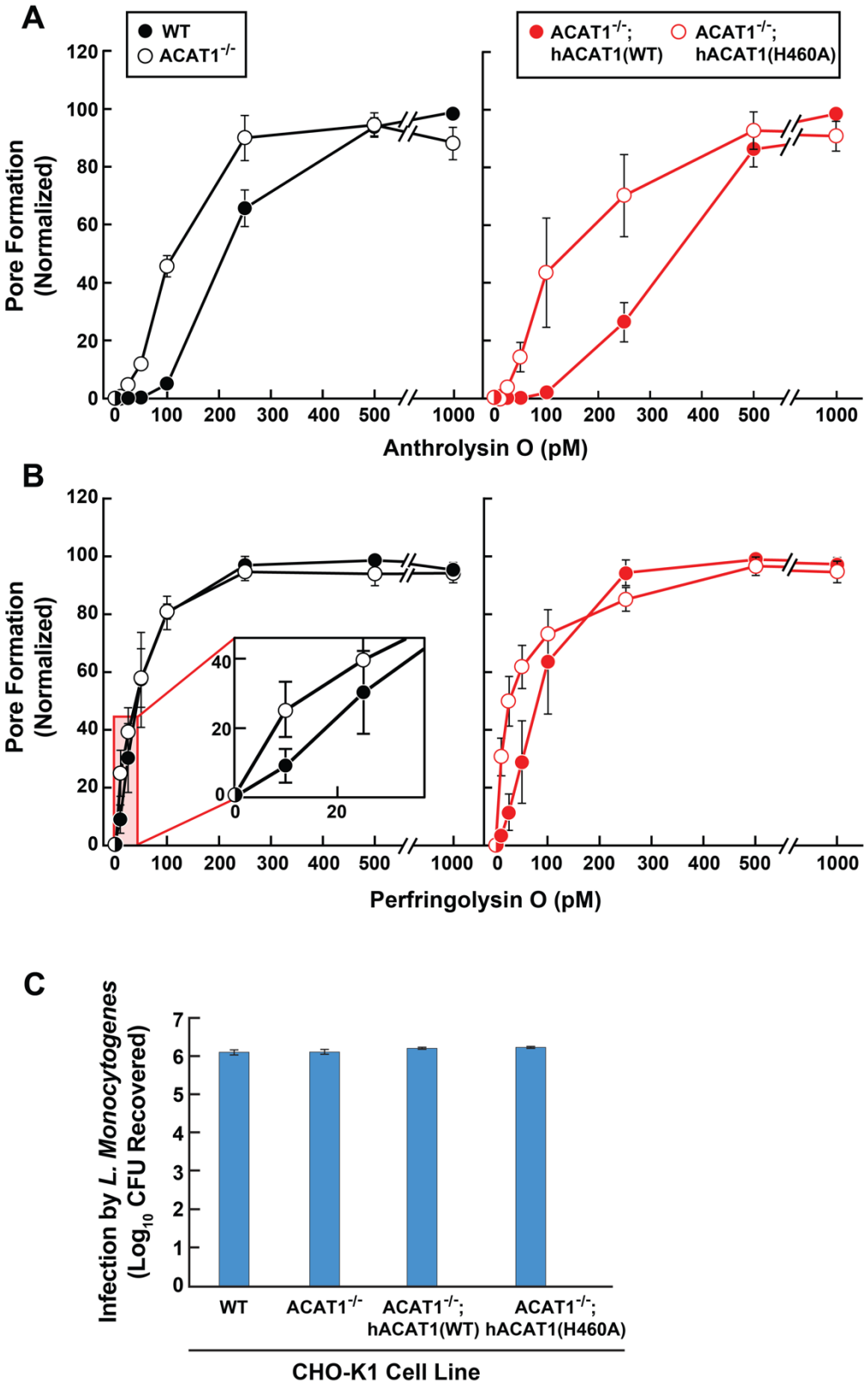

1524

Figure S6. Susceptibility of wild-type and ACAT-deficient CHO-K1 cells to pore formation by bacterial cytolysins and infection by *Listeria monocytogenes*.

(A, B) Pore formation by ALO and PFO. On day 0, the indicated versions of CHO-K1 cells were set up in medium B at a density of 7.5 x 10^4 cells per well of a 48-well plate. On day 1, media was removed, cells were washed twice with 500 µl of HBSS, followed by addition of 500 µl of HBSS supplemented with the indicated concentrations of His_6-ALO(FL) (A) or His_6-PFO(FL) (B). After incubation for 15 min at 37°C, media was removed, and pore formation was assessed as described in *Methods*. For each cell line, the maximum extent of pore formation for each replicate assay was set to 100%, and all other values were normalized to this set-point.

(C) Infection by *Listeria monocytogenes*. On day 0, the indicated versions of CHO-K1 cells were set up in medium I at a density of 1 x 10^5 cells per well of a 24-well plate. On day 1, cells were infected with *Listeria monocytogenes* (MOI = 1) for 90 min. Following this step, cells were washed twice with 1 ml of PBS followed by addition of 1 ml of medium I supplemented with 50 µg/ml of gentamicin. After 22 h, cells were harvested, and infection levels were determined as described in *Methods*.

Figure S7

A

Exon 6 of Huh7.5 ACAT1

Wild type sequence

```
5' - gtacctttctccccagGCTGGTGCTTGAGTTCAGCCTCCTGTCTTATGCTTTTGGCAAATTTCCTACCGTTGTTTGGACCTGGTGGATCATGTTCCTGTCTACATTT...CAGgtaaggtt
3' - catggaaaagaggggtgCGACCACGAACACAAGTCGGAGGACAGAATACGAAAACCGTTTAAAGGATGGCAAGAAACCTGGACCACCTAGTACAAGGACAGATGTAAA...GTCcattccaaa
AA: 176                L  V  L  E  F  S  L  L  S  Y  A  F  G  K  F  P  T  V  V  W  T  W  W  I  M  F  L  S  T  F     Q  260
```

Disrupted sequence #1 (1 bp insertion)

```
5' - gtacctttctccccagGCTGGTGCTTGAGTTCAGCCTCCTGTCTTATGCTTTTGGCAAATTTCCTACCGGTTGTTTGGACCTGGTGGATCATGTTCCTGTCTACATT
3' - catggaaaagaggggtgCGACCACGAACACAAGTCGGAGGACAGAATACGAAAACCGTTTAAAGGATGGCCAAGAAACCTGGACCACCTAGTACAAGGACAGATGTAA
AA: 176                L  V  L  E  F  S  L  L  S  Y  A  F  G  K  F  P  T  G  C  L  D  L  V  D  H  V  P  V  Y  I FSSLFSVSTLGHWL*
```

Disrupted sequence #2 (63 bp deletion)

```
5' - gtaccttGTTGTTTGGACCTGGTGGATCATGTTCCTGTCTACATTTTCAGTTCCCTATTTTCTGTTTCAACATTGGGCCACTGGCTATAGCAAGAGTTCTCATCCGCTGA
3' - catggaaCAACAAACCTGGACCACCTAGTACAAGGACAGATGTAAAAGTCAAGGGATAAAAGACAAAGTTGTAACCCGGTGACCGATATCGTTCTCAAGAGTAGGCCACT
AA: 176       L  F  G  P  G  G  S  C  S  C  L  H  F  Q  F  P  I  F  C  F  N  I  G  P  L  A  I  A  R  V  L  I  R  *
```

Exon 2 of Huh7.5 ACAT2

Wild type sequence

```
5' - cagGAAACACTGAGACGCACAGAGCCCCGGACTTGGTACAATGGACCCGACACATGGAGgtg
3' - gtcCTTTGTGACTCTGCGTGTCACGGGGCCTCAACCATGTTACCTGGGCTGTGTACCTCcac
AA: 29     N  T  E  T  H  R  A  P  D  L  V  Q  W  T  R  H  M  E
```

Disrupted sequence #1 (7 bp deletion)

```
5' - cagGAAACACTGAGACGCACAGAGCCCCGGACAATGGACCCGACACATGGAG
3' - gtcCTTTGTGACTCTGCGTGTCACGGGGCCTCTTACCTGGGCTGTGTACCTC
AA: 29     N  T  E  T  H  R  A  P  D  N  G  P  D  T  W  R  L*
```

Disrupted sequence #2 (1 bp insertion)

```
5' - cagGAAACACTGAGACGCACAGAGCCCCGGAACTTGGTACAATGGACCCGACACATGGA
3' - gtcCTTTGTGACTCTGCGTGTCACGGGGCCTTCAACCATGTTACCTGGGCTGTGTACCT
AA: 29     N  T  E  T  H  R  A  P  E  L  G  T  M  D  P  T  H  G GCEGTIAGASAGTTEGAAGSGHAGGYTILPITRQTSAPTSPRFLEQDPGAIPGETESFHHPQVPA*
```

B

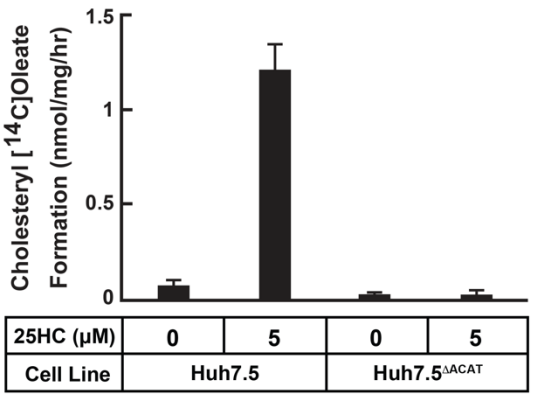

C

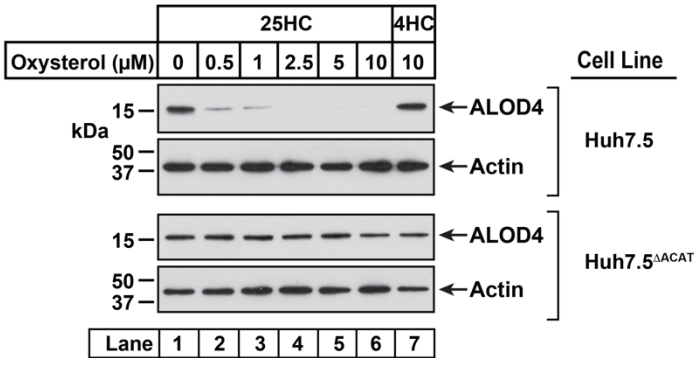

Figure S7. Characterization of a Huh7.5 cell line deficient in ACAT1 and ACAT2.

(A) Strategy for generating Huh7.5 cells deficient in ACAT1 and ACAT2. Guide RNAs were designed to target and disrupt exon 6 in human ACAT1 (also designated as SOAT1) and exon 2 in human ACAT2 (also designated as SOAT2). The 20-nucleotide target sequences are shown in green and the NGG PAM sequences are in purple. Genomic sequencing of the ACAT1 gene revealed a 1-bp insertion in one allele and a 63-bp deletion in the other allele that generated premature stop codons and truncated transcripts as indicated in red. Genomic sequencing of the ACAT2 gene revealed a 7-bp deletion in one allele and a 1-bp insertion in the other allele that generated premature stop codons and truncated transcripts as indicated in red.

(B) ACAT activity. On day 0, the indicated versions of Huh7.5 cells were set up in medium D at a density of 2.5 x 10^5 cells per 60-mm dish. On day 2, media was removed, cells were washed twice with 1 ml of PBS followed by addition of 2 ml of cholesterol-depleting medium (DMEM (high glucose) supplemented with 5% (v/v) LPDS, 50 μM compactin, 50 μM sodium mevalonate, 100 units/ml penicillin, and 100 μg/ml streptomycin sulfate). On day 3, media was removed, cells were washed with 1 ml of PBS followed by addition of 1 ml of the above cholesterol-depleting medium supplemented with the indicated concentration of 25HC. After incubation at 37°C for 1 h, each dish was supplemented with 0.2 mM sodium [^{14}C]oleate (6500 dpm/nmol) and incubated at 37°C for an additional 2 h, after which cells were harvested, and levels of cholesteryl [^{14}C]oleate were measured as described in *Methods*. Each column represents the mean of cholesterol esterification measurements from three experiments, and error bars show the standard error.

(C) Immunoblot analysis of ALOD4 binding. On day 0, the indicated versions of Huh7.5 cells were set up in medium D at a density of 1.5 x 10^5 cells per well of a 24-well plate. On day 1, media was removed, cells were washed twice with 500 μl of PBS followed by addition of 200 μl of medium D supplemented with the indicated concentrations of either 25HC or 4HC. After incubation at 37°C for 4 h, media was removed and replaced with 200 μl of medium D supplemented with 3 μM of His_6-Flag-ALOD4. After incubation at 37°C for 30 min, cells were washed twice with 500 μl of PBS, harvested, and equal aliquots of cell lysates were subjected to immunoblot analysis as described in *Methods*.